Electromagnetic Fixed Point and Flavor Transport

on the Rigid TFPT Branch

Stefan Hamann Alessandro Rizzo

Paper 3 of the TFPT 4.5 series – April 27, 2026

Abstract

This paper isolates the precision-readout layer of TFPT after the primitive kernel and carrier packet have been fixed. It treats the electromagnetic fixed point, the transport pole of the cusp cubic, the retained seed decoder, and the flavor transport grammar yielding α, δ_{ph}, λ_C, β_{rad}, Ω_b, θ_{13}, CKM, and PMNS readouts.

Scope box: inputs, contribution, non-claims, audit surface

Inputs from previous papers. Paper 1 supplies the primitive kernel and $[u_\Sigma] = 1$. Paper 2 supplies the rigid carrier, family count, admissible occupancy, compact Higgs index, and abelian index coefficient.

New theorem contribution. The electromagnetic fixed point, the transport pole, the retained seed decoder, and the UFE-form bridge to the determinant-line response:

$$\alpha^{-1}(0) = 137.035999216\ldots, \qquad P'(z) = 0 \Rightarrow \delta_{\mathrm{ph}}, \qquad \lambda_C = \sqrt{\varphi_0^{\mathrm{ret}}(1-\varphi_0^{\mathrm{ret}})}, \qquad \beta = \beta_{\mathrm{rad}}\frac{180^\circ}{\pi} \approx 0.2424^\circ,$$

and the structured local dyonic projection $\beta_{\mathrm{BH}}(r) \sim 16c_3^4 Q_e^{\mathrm{eff}} Q_m^{\mathrm{eff}}/r^2$ underlying the EHT-class achromatic residual intercept test.

Not claimed here. No full QFT closure, no gravity/metrology proof, no CMB, no E8, and no large pole-mass table.

Falsification or audit surface. The paper fails if any numerical constant enters after the fact, if α is used to tune later readouts, or if alternative discrete worlds are not visibly ruled out by the same branch constraints.

Claim contract

Claim. Exact electromagnetic fixed point and flavor/PMNS/CKM readouts on the rigid branch.
Inputs. Papers 1–2: primitive kernel, carrier packet, family count, Higgs index, abelian index.
First assumptions. Exact seam opening $\varphi_\Sigma(\alpha)$, transport pole, retained seed as UV shadow, branch budget 41.
Proof status. Bridge/readout layer with no-knobs audit.
Kill condition. Frozen inputs move after comparison, alternative discrete worlds survive, or precision rows fail stated tests.

Contents

1 Electromagnetic Closure

The electromagnetic calculation is presented only after the carrier branch is fixed. The fixed point is read as a closed-branch output:

$$\alpha^{-1}(0) = 137.035999216\ldots.$$

The paper should include the carrier form of the electromagnetic closure and the compact audit of which structural quantities enter the fixed point.

2 Transport Pole

The transport phase is governed by the cubic

$$P(z) = (z-1)\left(z-\frac{64}{729}\right)\left(z-\frac{1}{729}\right), \qquad P'(z) = 0.$$

The lower critical point determines δ_{ph} on the retained branch. The transport pole must be introduced as a branch consequence, not as a fit parameter.

3 Retained Seed Decoder

The retained seed

$$u := \varphi_0^{\mathrm{ret}}$$

projects to the bridge observables

$$\lambda_C = \sqrt{\varphi_0^{\mathrm{ret}}(1-\varphi_0^{\mathrm{ret}})}, \qquad \beta_{\mathrm{rad}} = \frac{\varphi_0^{\mathrm{ret}}}{4\pi}, \qquad \sin^2\theta_{13} = \varphi_0^{\mathrm{ret}} e^{-\gamma}.$$

The text should make explicit which earlier theorem fixes each symbol before it appears in a readout.

3.1 Compact UFE bridge for the birefringence seed

Before the determinant-line response is invoked in its full form, the same retained seed admits a short bridge derivation that connects the boundary-normalised axion–photon coupling to the cosmological birefringence amplitude. Starting from the unified-field-equation reduction of the seam transfer, the dimensionless axion–photon anomaly coefficient is

$$g_{a\gamma\gamma} = -4\,c_3 = -\frac{1}{2\pi},$$

and the modified Maxwell sector responds to a constant axion increment $\Delta a = \varphi_0^{\mathrm{ret}}$ on the admissible branch. The local rotation rate per unit determinant-line phase is then

$$\beta = 2\,c_3\,\Delta a,$$

so substituting $\Delta a = \varphi_0^{\mathrm{ret}}$ and $c_3 = \frac{1}{8\pi}$ recovers the seed identity

$$\beta_{\mathrm{rad}} = \frac{\varphi_0^{\mathrm{ret}}}{4\pi}, \qquad \beta = \beta_{\mathrm{rad}} \times \frac{180^\circ}{\pi} \approx 0.2424^\circ. \tag{1}$$

This compact reduction is intended as a reader bridge; the determinant-line / Chern–Simons formulation of Paper 3 and Paper 4 remains the load-bearing derivation.

Remark (Achromatic, dyonic intercept and the α-kernel). The same admissibility data emits a structured *local* astrophysical β amplitude in the magnetised inflow region of a compact object,

$$\beta_{\mathrm{BH}}(r) \sim \frac{Q_e^{\mathrm{eff}}\,Q_m^{\mathrm{eff}}}{256\pi^4\,r^2} = 16\,c_3^4\,\frac{Q_e^{\mathrm{eff}}\,Q_m^{\mathrm{eff}}}{r^2} = \frac{\delta_{\mathrm{top}}}{3}\,\frac{Q_e^{\mathrm{eff}}\,Q_m^{\mathrm{eff}}}{r^2}, \tag{2}$$

where $\delta_{\mathrm{top}} = 48c_3^4$ is the same topological coefficient that controls the precision-zone correction of the α-kernel. The corresponding observation channel is the achromatic *residual intercept* of the linear-polarization angle in horizon-scale polarimetry,

$$\chi_0^{\mathrm{res}}(x) = \chi_0^{\mathrm{obs}}(x) - \chi_0^{\mathrm{GRMHD}}(x),$$

i.e. the part of χ_0 left after the GRMHD/synchrotron forward model and calibration are subtracted. The TFPT contribution is the structured component of $\chi_0^{\mathrm{res}}(x)$ with the spatial $1/r^2$ profile of (2) and a sign flip under reversal of the effective $E\cdot B$ orientation. The coupling $1/(256\pi^4)$ is fixed; the geometric weights $Q_e^{\mathrm{eff}}(x), Q_m^{\mathrm{eff}}(x)$ and the emission radius are model dependent. A dedicated standalone prediction note states the full observation protocol and three independent null tests (frequency, spatial profile, sign flip).

4 Flavor Transport

The CKM and PMNS closure block belongs here, together with the transport grammar and regularized Yukawa kernels needed for the flavor statements. Representative hard readouts include

$$|V_{ub}| = \frac{|V_{us}|^3}{3}.$$

Large mass tables belong in the companion or a later empirical ledger, not in this paper.

5 No-Knobs Audit

Constant	First appearance	Prior dependency	Before α?	Variation consequence
Y	Paper 2 carrier theorem	Paper 1 primitive kernel	Yes	Breaks $3+2$, gauge quotient, and all downstream readouts.
$[u_\Sigma]$	Paper 1 seam generator	Boundary primitive kernel	Yes	Breaks family counting and transport branch normalization.
φ_0^{ret}	Transport branch	Papers 1–2	Yes	Moves λ_C, β_{rad}, θ_{13}, and flavor transport together.
N_Φ	Paper 2 Higgs index	Carrier/Higgs discharge	Yes	Changes the electromagnetic budget.
b_1	Paper 2 abelian index	Carrier packet	Yes	Changes the fixed-point coefficient.

6 Alternative Discrete Worlds

The alternative discrete worlds table is a falsification device. It should not be presented as decorative numerics. Each alternative must fail because it breaks a prior branch constraint, the fixed-point equation, or the simultaneous reuse audit.

7 Main Technical Development

This section contains the main technical development assigned to this paper by the TFPT 4.5 clean split. Cross-paper background is referenced through dependency and scope boxes; extended backend material is kept in the Technical Companion.

8 Kernel numerics and electromagnetic closure

The boundary-to-carrier presentation should not leave the impression that TFPT is hard only at the level of group theory and representation bookkeeping. The numerical kernel already fixes a nontrivial output layer. Here that layer is pulled forward and read as the first established output package of the carrier/output architecture rather than as a later list of disconnected constants.

Theorem 8.1 (Primitive seam generator)**.** *The primitive relative seam loop defines the positive generator*

$$[u_\Sigma] = 1 \in K^1(S^1) \cong \mathbb{Z}.$$

Hence the associated seam spectral flow is

$$SF(U_\Sigma) = 1, \qquad \Delta_\Sigma = 2\pi.$$

In the relative Chern normalization, the seam constant is

$$c_3 := \frac{\Delta_\Sigma}{16\pi^2} = \frac{1}{8\pi}.$$

Moreover the seam-even base opening is the normalized complement of the carrier quadratic norm,

$$\varphi_{\text{base}} := \frac{1-\gamma}{\pi} = \frac{1-\operatorname{Tr}_E Y^2}{\pi} = \frac{1}{6\pi}.$$

Proof sketch. The primitive reconstruction yields one elementary relative seam class and therefore one primitive generator of the seam K^1 lattice. Along a single positive seam circuit the spectral flow changes by one, so the associated loop has class $[u_\Sigma] = 1$ and spectral flow $SF(U_\Sigma) = 1$. The primitive circuit closes after one full turn, giving $\Delta_\Sigma = 2\pi$ and hence $c_3 = \Delta_\Sigma/(16\pi^2) = 1/(8\pi)$. The carrier theorem gives $\gamma = \operatorname{Tr}_E Y^2 = 5/6$, so the seam-even opening is the normalized complement of the carrier quadratic norm rather than a new independent numerical input. □

Remark (Interpretive picture of the primitive start state)*.* At the level of physical intuition, the primitive spectral seed may be read as a minimal nontrivial relative defect state: two sheets, one seam, one elementary relative winding, and an undecomposed internal rank-5 kernel before the carrier split is imposed. This is only an interpretive picture, not a new theorem. Its role is to explain why the earliest hard numbers $(c_3, \varphi_{\text{base}})$ already look like seam-normalized responses of a genuinely relative starting configuration.

8.1 Carrier form of the electromagnetic closure

At this stage the electromagnetic closure is kept in generic closed form. The hard carrier data fix

$$c_3 = \frac{1}{8\pi}, \qquad \varphi_{\text{base}} = \frac{1}{6\pi},$$

while the later family and Higgs theorems will specialize the abelian index coefficient and the topological bridge coefficient.

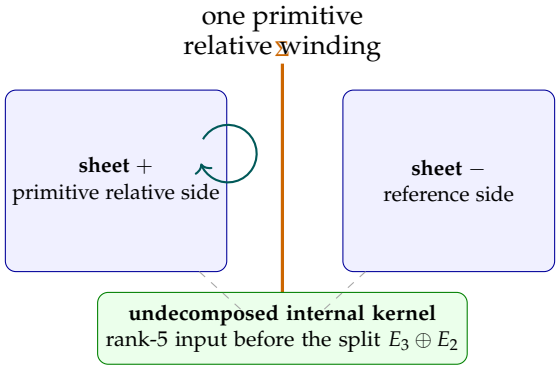

Figure 1. Interpretive primitive start sketch. Two sheets, one seam, one elementary relative winding, and an undecomposed rank-5 kernel appear before the later split into $E_3 \oplus E_2$. The picture is heuristic only; the theorem-level data are reconstructed from the one-sided boundary datum.

Proposition 8.2 (Carrier susceptibility exponent)**.** On the minimal carrier branch,

$$B\gamma = \frac{3}{2} \cdot \frac{5}{6} = \frac{5}{4}.$$

Definition 8.3 (Minimal primitive seam transfer)**.** Let ψ_Σ be the normalized primitive seam mode singled out by [TFPT cross-reference: `thm:primitive-seam-generator`]. Define the minimal seam transfer operator by the rank-one projector

$$U_\Sigma^{\min} := |\psi_\Sigma\rangle\langle\psi_\Sigma|.$$

With

$$q(\alpha) := \delta_{\mathrm{top}} e^{-2\alpha}, \qquad B\gamma = \frac{5}{4},$$

one has

$$\mathcal{W}_\Sigma(\alpha) := -B\gamma \, \mathrm{Tr}_{\mathrm{adm}} \log\bigl(1 - q(\alpha) U_\Sigma^{\min}\bigr) = -\frac{5}{4} \log(1 - q(\alpha)).$$

$$\mathcal{T}_\Sigma(\alpha) = e^{\mathcal{W}_\Sigma(\alpha)} = (1 - q(\alpha))^{-5/4}.$$

$$\varphi_\Sigma(\alpha) = \varphi_{\mathrm{base}} + q(\alpha)(1 - q(\alpha))^{-5/4}. \tag{3}$$

Proposition 8.4 (Normalized scalar closure potential)**.** Let

$$F_{U(1)}(\alpha) := \alpha^3 - 2c_3^3\alpha^2 - 8c_3^6 b_1 \log\bigl(\varphi_\Sigma(\alpha)^{-1}\bigr).$$

There exists a unique quartic local counterterm P_{loc} satisfying

$$P_{\mathrm{loc}}(0) = P'_{\mathrm{loc}}(0) = 0, \qquad P'_{\mathrm{loc}}(\alpha) = \alpha^3 - 2c_3^3\alpha^2,$$

namely

$$P_{\mathrm{loc}}(\alpha) = \frac{\alpha^4}{4} - \frac{2}{3}c_3^3\alpha^3.$$

Hence the normalized scalar closure potential

$$\Gamma_{U(1)}(\alpha) := \frac{\alpha^4}{4} - \frac{2}{3}c_3^3\alpha^3 - 8c_3^6 b_1 \int_0^\alpha \log\bigl(\varphi_\Sigma(a)^{-1}\bigr)\, da$$

satisfies

$$\partial_\alpha \Gamma_{U(1)}(\alpha) = F_{U(1)}(\alpha).$$

Theorem 8.5 (Exact electromagnetic closure on the minimal seam mode)**.** *On the canonical branch one has*

$$c_3 = \frac{1}{8\pi}, \qquad \varphi_{\mathrm{base}} = \frac{1}{6\pi}, \qquad \delta_{\mathrm{top}} = \frac{3}{256\pi^4}, \qquad \sum_{f,j} L_{f,j}^{\mathrm{diag}} + N_\Phi = 40 + 1 = 41.$$

With the rank-one seam transfer of Definition 8.3, the closure equation is the scalar equation

$$F_{U(1)}(\alpha) = 0, \qquad F_{U(1)}(\alpha) = \alpha^3 - 2c_3^3\alpha^2 - \frac{4}{5}c_3^6\left(\sum_{f,j} L_{f,j}^{\mathrm{diag}} + N_\Phi\right)\log\bigl(\varphi_\Sigma(\alpha)^{-1}\bigr), \tag{4}$$

where

$$\varphi_\Sigma(\alpha) = \frac{1}{6\pi} + \frac{3e^{-2\alpha}}{256\pi^4}\left(1 - \frac{3e^{-2\alpha}}{256\pi^4}\right)^{-5/4}.$$

This equation has a unique positive root

$$\alpha_\star = 0.00729735256220985312786969108226575414\ldots$$

and therefore

$$\alpha_\star^{-1} = 137.03599216840712503537860303803880 37\ldots.$$

Proof. The explicit formulas above follow from the rank-one determinant identity

$$\det(1 - qU_\Sigma^{\mathrm{min}}) = 1 - q \qquad \text{for } U_\Sigma^{\mathrm{min}} = |\psi_\Sigma\rangle\langle\psi_\Sigma|.$$

The derivative of the closure function is

$$F'_{U(1)}(\alpha) := 3\alpha^2 - 4c_3^3\alpha - \frac{8}{5}c_3^6\left(\sum_{f,j} L_{f,j}^{\mathrm{diag}} + N_\Phi\right)\frac{q(\alpha)(1-q(\alpha))^{-9/4}\bigl(1+q(\alpha)/4\bigr)}{\varphi_{\mathrm{base}} + q(\alpha)(1-q(\alpha))^{-5/4}}.$$

On $[0, 2\cdot 10^{-4}]$ one verifies by interval arithmetic that

$$F_{U(1)}(\alpha) < 0.$$

On $[2\cdot 10^{-4}, 10^{-1}]$ one verifies by interval arithmetic that

$$F'_{U(1)}(\alpha) > 0.$$

Finally

$$F_{U(1)}(10^{-2}) > 0.$$

Therefore $F_{U(1)}$ crosses zero exactly once. The displayed numerical root is obtained by monotone bisection on that interval. □

Remark (Asymptotic opening as a secondary expansion). Using Proposition 8.2, the determinant output admits the small opening expansion

$$\varphi_\Sigma(\alpha) = \varphi_{\mathrm{base}} + \delta_{\mathrm{top}}e^{-2\alpha} + \frac{5}{4}\delta_{\mathrm{top}}^2 e^{-4\alpha} + O(e^{-6\alpha}),$$

which should be read only as a secondary expansion of the determinant output, not as the primary definition of the electromagnetic closure.

The dependency structure of the electromagnetic closure is displayed in Figure 2. What matters is not one formula in isolation, but the fact that the same carrier-side inputs fix the rank-one determinant, the scalar closure potential, and the fixed-point equation in one direction. The later transport and Higgs theorems then specialize the budget $\sum_{f,j} L_{f,j}^{\mathrm{diag}} + N_\Phi$ and δ_{top} to their canonical closed values.

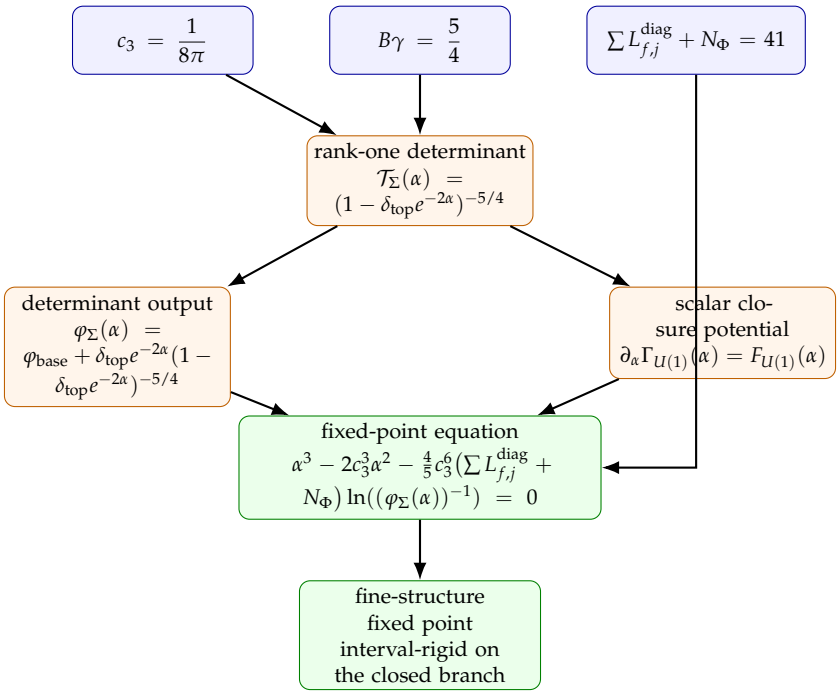

Figure 2. α closure flow in closed form. The carrier data determine the rank-one determinant, the scalar closure potential, and the fixed-point equation. The numerical specialization is made only after the transport and Higgs theorems close the branch budget.

Remark (Logarithmic scale closure of the electromagnetic equation). Define the internally generated logarithmic scale

$$\mu_\Sigma(\alpha) := (\varphi_\Sigma(\alpha))^{-1}.$$

Then [TFPT cross-reference: `eq:carrier-cfe`] is equivalent to

$$\ln \mu_\Sigma(\alpha) = \frac{\alpha^2(\alpha - 2c_3^3)}{\frac{4}{5}c_3^6\left(\sum_{f,j} L_{f,j}^{\mathrm{diag}} + N_\Phi\right)}.$$

Thus the observed fine-structure constant is selected by a balance between a geometric cubic term and a self-generated logarithmic scale parameter. This is RG-like and transmutation-like, because the coefficient is the internally closed transport-plus-Higgs budget divided by 10, and the logarithm is attached to an internally produced scale. In the present paper it should be read as *logarithmic scale closure* or a geometric fixed-point equation rather than as an externally prescribed one-loop running law. The symbol $\mu_\Sigma(\alpha)$ here is local to the electromagnetic closure discussion and should not be confused with the later matching scale M_Σ.

A related appendix continuation records that with

$$g := 5, \qquad d := \dim \mathfrak{g}_{\mathrm{SM}} = 12,$$

$$\gcd(\Omega_{\mathrm{adm}}, D_{\mathrm{start}}) = d, \qquad \mathrm{lcm}(\Omega_{\mathrm{adm}}, D_{\mathrm{start}}) = g(g-1)d = 240 = |R(E_8)|.$$

8.2 Kernel output package

The benchmark row for $\alpha^{-1}(0)$ is defined by the positive self-consistent root of [TFPT cross-reference: `eq:carrier-cfe`], not by freezing the opening at its retained seed value. On the canonical branch that positive root remains

$$\alpha^{-1}(0) = 137.035\,999\,216\,840\,71.$$

For the remaining one-seed relations we keep the retained branch opening

$$c_3 = \frac{1}{8\pi}, \qquad \varphi_0^{\mathrm{ret}} = \frac{1}{6\pi} + \frac{3}{256\pi^4}, \tag{5}$$

Remark (Exact opening versus retained seed). The two symbols belong to the same admissible branch but play different jobs. The electromagnetic α row uses the exact seam generating function $\varphi_\Sigma(\alpha)$ inside the carrier-form closure equation, whereas the one-seed bridge relations freeze that branch to the retained canonical seed φ_0^{ret}. Thus $\varphi_\Sigma(\alpha)$ belongs only to the exact α benchmark line, while φ_0^{ret} is the seed used for $(\beta_{\mathrm{rad}}, \Omega_b, \lambda_C, \sin^2\theta_{13})$.

and the same retained kernel package emits the compact seed chain

$$\begin{aligned} C_{a\gamma\gamma} = -4c_3 = -\frac{1}{2\pi}, \quad \beta_{\mathrm{rad}} &= \frac{\varphi_0^{\mathrm{ret}}}{4\pi}, \\ \Omega_b = (4\pi - 1)\beta_{\mathrm{rad}}, \qquad \lambda_C &= \sqrt{\varphi_0^{\mathrm{ret}}(1 - \varphi_0^{\mathrm{ret}})}, \\ \sin^2\theta_{13} = \varphi_0^{\mathrm{ret}} e^{-\gamma}. & \end{aligned} \tag{6}$$

Remark (Why the α row must stay self-consistent). The exact self-consistent equation with $\varphi_\Sigma(\alpha)$ yields the benchmark value

$$\alpha^{-1}(0) = 137.035\,999\,216\,840\,71.$$

Its second-order truncation reproduces the first two correction coefficients, but it is not itself the benchmark definition. If one instead freezes the opening at

$$\varphi_0^{\mathrm{ret}} = \frac{1}{6\pi} + \frac{3}{256\pi^4},$$

the root shifts to $\alpha^{-1}(0) \approx 137.036\,501\,465$, i.e. by about 5.02×10^{-4}, which is roughly $2.4 \times 10^4 \sigma$ on the CODATA/NIST uncertainty. The wording of the α benchmark must therefore remain explicit: the benchmark uses the exact seam generating function, while the quadratic formula is only its controlled asymptotic shadow.

Kernel-output package

The point of this section is not to claim more numerics than TFPT currently owns. It is to show that the established kernel already fixes a coherent electromagnetic package before the later completion theorems begin: the seam constant c_3, the retained canonical seed φ_0^{ret}, the self-consistent carrier-form CFE for α, the dimensionless axion–photon anomaly coefficient, the birefringence seed, and the Cabibbo anchor.

8.3 UV seed-shadow identities and the Cabibbo inversion

The retained scalar seed φ_0^{ret} still satisfies exact UV identities. In the present version these identities are auxiliary kernel bookkeeping rather than the independence grammar of the physical observable layer. In particular, the Cabibbo angle admits an explicit inversion back to the UV seed:

$$\varphi_0^{\mathrm{ret}} = \frac{1 - \sqrt{1 - 4\lambda_C^2}}{2}. \tag{7}$$

Remark (Catalan expansion of the Cabibbo inversion). Setting

$$x := \lambda_C^2,$$

the inversion formula becomes

$$\varphi_0^{\mathrm{ret}} = x\,C(x), \qquad C(x) := \frac{1-\sqrt{1-4x}}{2x}.$$

Hence

$$\varphi_0^{\mathrm{ret}} = \sum_{n\geq 0} C_n\,\lambda_C^{2n+2} = \lambda_C^2 + \lambda_C^4 + 2\lambda_C^6 + 5\lambda_C^8 + 14\lambda_C^{10} + \cdots, \tag{8}$$

where C_n are the Catalan numbers. In the present paper the appropriate interpretation of this identity is noncrossing combinatorics on the seed side; it is a theorem-level strengthening of the one-seed compression rather than a claim about planar Feynman graphs, a specific large-N / 't Hooft resummation, or a holographic flavor limit.

Proposition 8.6 (Retained seed as one decoder)**.** Set

$$u := \varphi_0^{\mathrm{ret}}.$$

On the retained branch one has

$$\lambda_C^2 = u(1-u), \qquad \beta_{\mathrm{rad}} = \frac{u}{4\pi}, \qquad \Omega_b = \left(1-\frac{1}{4\pi}\right)u, \qquad \sin^2\theta_{13} = e^{-\gamma}u.$$

Equivalently,

$$u = \frac{1-\sqrt{1-4\lambda_C^2}}{2} = 4\pi\beta_{\mathrm{rad}} = \frac{\Omega_b}{1-\frac{1}{4\pi}} = e^{\gamma}\sin^2\theta_{13}.$$

Thus the retained branch carries a single decoder

$$u \longmapsto (\lambda_C, \beta_{\mathrm{rad}}, \Omega_b, \theta_{13}).$$

Proof. The forward identities are exactly the retained-seed bridge relations. The inverse identities follow from the Cabibbo inversion [TFPT equation: `eq:cabibbo-inversion`] and direct elimination of u from the same four formulas. □

Eliminating the retained seed through the Cabibbo inversion gives the equivalent λ_C-only formulas:

$$\begin{aligned} \beta_{\mathrm{rad}} &= \frac{1-\sqrt{1-4\lambda_C^2}}{8\pi}, \\ \Omega_b &= \frac{4\pi-1}{8\pi}\left(1-\sqrt{1-4\lambda_C^2}\right), \\ \sin^2\theta_{13} &= \frac{e^{-\gamma}}{2}\left(1-\sqrt{1-4\lambda_C^2}\right). \end{aligned} \tag{9}$$

Corollary 8.7 (Vacuum half-circle and UV-angle parametrization)**.** *On the retained UV seed split one has the exact identity*

$$\lambda_C^2 + \left(\varphi_0^{\mathrm{ret}} - \frac{1}{2}\right)^2 = \frac{1}{4}.$$

Defining

$$\sin^2\theta_{\mathrm{UV}} := \varphi_0^{\mathrm{ret}},$$

one obtains

$$\lambda_C = \frac{1}{2}\sin(2\theta_{\mathrm{UV}}), \qquad \sin^2\theta_{13} = e^{-\gamma}\sin^2\theta_{\mathrm{UV}}, \qquad \Omega_b = \left(1-\frac{1}{4\pi}\right)\sin^2\theta_{\mathrm{UV}}.$$

Proof. The exact seed relation $\lambda_C^2 = \varphi_0^{\mathrm{ret}}(1-\varphi_0^{\mathrm{ret}})$ is equivalent to the displayed half-circle identity after completing the square. The θ_{UV} parametrization then follows immediately from $\sin^2\theta_{\mathrm{UV}} = \varphi_0^{\mathrm{ret}}$ together with the exact retained-seed formulas for $\sin^2\theta_{13}$ and Ω_b. □

Corollary 8.8 (CKM–PMNS bridge law)**.** *On the closed branch one has the exact relation*

$$\sin^2\theta_{13} = \frac{e^{-5/6}}{2}\left(1-\sqrt{1-4\lambda_C^2}\right).$$

Equivalently,

$$\lambda_C^2 = e^{5/6}\sin^2\theta_{13} - e^{10/6}\sin^4\theta_{13}.$$

In internal branch form,

$$\sin^2\theta_{13} = 0.0231084351588811\ldots$$

with no additional fit parameter.

Proof. By [TFPT cross-reference: `eq:cabibbo-inversion`],

$$\varphi_0^{\mathrm{ret}} = \frac{1-\sqrt{1-4\lambda_C^2}}{2}.$$

By the exact seed identity,

$$\sin^2\theta_{13} = \varphi_0^{\mathrm{ret}} e^{-\gamma}, \qquad \gamma = \frac{5}{6}.$$

Substituting φ_0^{ret} gives the displayed formula. □

Corollary 8.9 (Baryon–reactor bridge law)**.** *On the closed branch one has the exact cross-sector relation*

$$\Omega_b = \left(1-\frac{1}{4\pi}\right)e^{5/6}\sin^2\theta_{13} = \frac{4\pi-1}{8\pi}\left(1-\sqrt{1-4\lambda_C^2}\right).$$

In internal branch form,

$$\Omega_b = 0.0489406626654501\ldots$$

with no additional fit parameter.

Proof. The exact seed-budget identities give

$$\Omega_b = (4\pi-1)\beta_{\mathrm{rad}}, \qquad \beta_{\mathrm{rad}} = \frac{\varphi_0^{\mathrm{ret}}}{4\pi}, \qquad \sin^2\theta_{13} = \varphi_0^{\mathrm{ret}} e^{-5/6}.$$

Eliminating φ_0^{ret} yields the displayed cross-sector identity. Eliminating φ_0^{ret} instead through [TFPT cross-reference: `eq:cabibbo-inversion`] gives the equivalent λ_C form. □

Corollary 8.10 (Matter-radiation quotient on the retained seed split)**.** *On the retained seed split one has the exact quotient identity*

$$\frac{\Omega_b}{\beta_{\mathrm{rad}}} = 4\pi - 1.$$

Proof. This is the direct quotient of the exact retained-seed identities

$$\Omega_b = (4\pi-1)\beta_{\mathrm{rad}}, \qquad \beta_{\mathrm{rad}} = \frac{\varphi_0^{\mathrm{ret}}}{4\pi}.$$

□

Remark (Interpretive reading of the retained seed split). The same one-seed decoder carries the exact budget identity

$$\Omega_b + \beta_{\mathrm{rad}} = \varphi_0^{\mathrm{ret}}. \tag{10}$$

Indeed,

$$\Omega_b + \beta_{\mathrm{rad}} = (4\pi - 1)\beta_{\mathrm{rad}} + \beta_{\mathrm{rad}} = 4\pi\,\beta_{\mathrm{rad}} = \varphi_0^{\mathrm{ret}}.$$

Both [TFPT cross-reference: `cor:matter-radiation-quotient,eq:seed-budget-identity`] are exact retained-seed identities. Any solid-angle or spherical-surface interpretation remains interpretive and is not used as theorem input.

Thus on the canonical branch, β, Ω_b, λ_C, and θ_{13} are four exact projections of the same retained decoder $u = \varphi_0^{\mathrm{ret}}$. Conversely, θ_{13} fixes λ_C and Ω_b through $\varphi_0^{\mathrm{ret}} = e^{\gamma}\sin^2\theta_{13}$. This is the derived-consequence layer of the retained seed split, not a separate independent theorem surface.

8.4 Carrier comparison of alternative discrete worlds

The strongest numerical pressure test on the carrier packet is not a further precision hit. It is that nearby wrong discrete worlds miss the electromagnetic closure decisively.

Proposition 8.11 (Numerical comparison of alternative discrete worlds)**.** Let

$$\alpha^{-1}(0; N_{\mathrm{fam}}, N_\Phi, \nu^c)$$

denote the positive self-consistent root of the carrier-form electromagnetic closure equation [TFPT equation: `eq:carrier-cfe`] for the indicated discrete data. Then:

Discrete world	Change from canonical	$\alpha^{-1}(0)$	Residual vs CODATA	Reading
canonical $(3, 1, \mathbf{yes})$	—	137.0359992	$+3.9\times10^{-8}$	inside CODATA window ($+1.87\sigma$)
$N_{\mathrm{fam}} = 2$	one family fewer	156.094	$+19.1$	catastrophically excluded
$N_{\mathrm{fam}} = 4$	one family more	124.835	-12.2	catastrophically excluded
$N_\Phi = 2$	two light Higgs doublets	135.946	-1.09	catastrophically excluded
no ν^c	remove right-handed neutrino	137.0338	-2.16×10^{-3}	excluded ($\sim1.03\times10^5\sigma$)

Proof sketch. Hold fixed

$$c_3 = \frac{1}{8\pi}, \qquad \varphi_{\mathrm{base}} = \frac{1}{6\pi}, \qquad \gamma = \frac{5}{6}, \qquad B = \frac{3}{2},$$

and solve the positive self-consistent root of the same scalar closure equation on each discrete world:

$$\alpha^3 - 2c_3^3\alpha^2 - 8c_3^6\, b_1(N_{\mathrm{fam}}, N_\Phi)\ln\!\big(\varphi_\Sigma(\alpha)^{-1}\big) = 0,$$

with

$$\varphi_\Sigma(\alpha) = \varphi_{\mathrm{base}} + \delta_{\mathrm{top}}e^{-2\alpha}(1 - \delta_{\mathrm{top}}e^{-2\alpha})^{-5/4}, \qquad \delta_{\mathrm{top}} = \Omega_{\mathrm{adm}}c_3^4, \qquad \delta_2 = \frac{5}{4}\,\delta_{\mathrm{top}}^2,$$

and

$$b_1(N_{\mathrm{fam}}, N_\Phi) = \frac{4}{3}N_{\mathrm{fam}} + \frac{1}{10}N_\Phi.$$

For the no-ν^c row, b_1 stays unchanged because $Y(\nu^c) = 0$, while the occupancy changes from $\Omega_{\mathrm{adm}} = 48$ to $\Omega_{\mathrm{adm}} = 45$ because the one-family packet drops from 16 to 15 states. The same positive-branch solver and tolerance are used for every row, so the deviations are arithmetic consequences of changed discrete data rather than fits. □

discrete world	Residual vs CODATA	reading
canonical $(3, 1, \text{yes})$	$+3.9 \times 10^{-8}$	inside the CODATA window
$N_{\text{fam}} = 2$	$+19.1$	catastrophically excluded
$N_{\text{fam}} = 4$	-12.2	catastrophically excluded
$N_{\Phi} = 2$	-1.09	extra light doublet breaks closure
no ν^c	-2.16×10^{-3}	$\sim 1.03 \times 10^5 \sigma$ exclusion

Figure 3. Comparison matrix for alternative discrete worlds. The middle column records the residual versus the CODATA benchmark rather than a misleading shift relative to the canonical row. Once the discrete packet is changed, the electromagnetic closure leaves the observed window decisively.

Remark. Two families shift α^{-1} by $+19$, four families by -12, and two Higgs doublets by -1.09. Even the mildest alternative—removing ν^c—shifts the value by 2.16×10^{-3}, which is $\sim 1.03 \times 10^5$ times the CODATA uncertainty. This is therefore a useful comparison pressure test on the canonical branch rather than an additional theorem in the reconstruction chain.

9 Closure architecture B: Yukawas, masses, flavor, hadronic admissibility, and the strong-CP sector

The second closure-architecture block is the transport closure. Its role is to turn the carrier packet and the family/occupancy closure into actual masses, mixings, hadronic admissibility, and control of the strong-CP sector. The logic is again staged: first the discrete phase operator and the transport kernel, then residue and winding data, then matrix-factorized Yukawas, hadronic selection, determinant-line phase extraction, and finally the strong-CP closure theorem.

9.1 Discrete phase operator and transport grammar

Let

$$\omega = e^{2\pi i/3}, \qquad U_6 = \operatorname{diag}(1, \omega, \omega^2, -1, -\omega, -\omega^2).$$

This makes the phase grammar concrete rather than rhetorical. The six admissible phases are shown as a finite hexagonal transport geometry in Figure 4: the cusp values live on the same real axis as the positive-real phase, the admissible gap is visible directly, and the holonomy phase can be read as a triangle on the same discrete transport base.

Remark (Hexagonal spectral geometry). The operator U_6 is a unitary circulant with eigenphases $e^{in\pi/3}$ for $n = 0, \ldots, 5$ and is unitarily equivalent to the one-step translation operator on a six-site ring. The transport kernel $D_y = y\,\mathbf{1} - \delta_{\text{ph}} U_6$ is therefore the resolvent denominator of a finite quantum walk, equivalently a tight-binding transfer problem, on the discrete C_6 cycle. The regularized inverse introduced below plays the role of the corresponding Green kernel. CKM and PMNS mixings, mass hierarchies, and the Möbius quotients of Equation (16) are thus not loose analytic fits but spectral-theory statements on a regular hexagon. The near-pole hierarchy at $y \approx \delta_{\text{ph}}$ becomes the resonance of a hexagonal resolvent rather than tuned parameter choice.

The family-side holonomy phase is separated in Figure 5 so that the transport base and the flavor readout remain visually distinct.

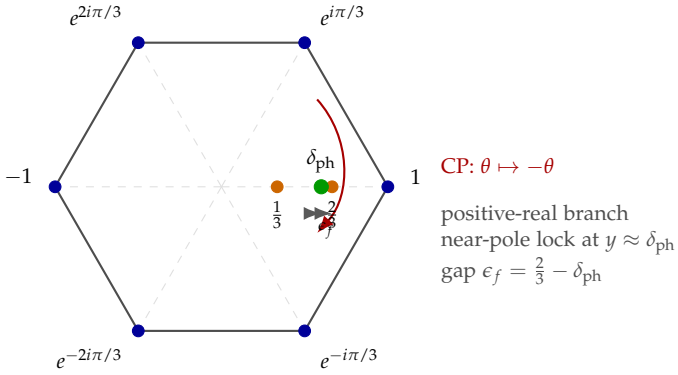

Figure 4. Finite transport geometry on the hexagon C_6. The six U_6 phases form the discrete transport base, while the admissible cusps $y \in \{1, \frac{1}{3}, \frac{2}{3}\}$ and the branch pole δ_{ph} lie on the positive-real axis with gap $\epsilon_f = \frac{2}{3} - \delta_{\mathrm{ph}}$.

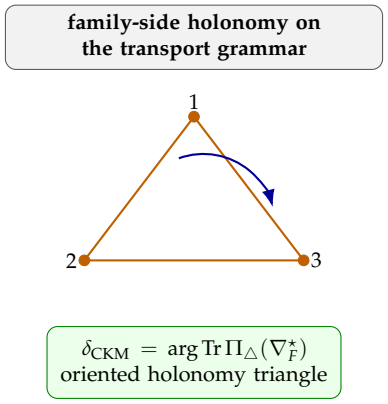

Figure 5. Holonomy triangle on the same discrete transport grammar. The CKM phase is read as the oriented three-cycle phase $\delta_{\mathrm{CKM}} = \arg \mathrm{Tr}\, \Pi_{\triangle}(\nabla_F^{\star})$ rather than as an additional transport parameter.

9.2 Regularized Yukawa kernels and path-length masses

$$P_{\mathrm{str}} := P_{\Sigma,+} P_{\mathrm{sing}} P_{\Theta}, \qquad P_{\Sigma,+} := \frac{\mathbf{1} + \iota_{\mathrm{C}}}{2}, \qquad P_{\Theta} := \frac{1}{2}(\mathbf{1} + Q_{\Theta}), \qquad P_{\mathrm{sing}} := \frac{1}{3}(\mathbf{1} + Z_c + Z_c^2).$$

Definition 9.1 (Structural transport kernel)**.** For each fermion sector define the structural positive transport kernel by

$$K_f^{\mathrm{str}} := \left(P_{\mathrm{str}} D_f^{\dagger} D_f P_{\mathrm{str}}\right)^{-1/2},$$

whenever the inverse exists on $\mathrm{Ran}(P_{\mathrm{str}})$. The final admissible kernel is the restriction of this operator to the gap-stable branch selected below. The transport pole δ_{ph} is fixed by the structural stationarity of the exact determinant functional

$$\mathcal{F}_{\mathrm{tr}}(\delta) := \sum_{y \in \{1, 1/3, 2/3\}} \left[-\log \det\left(D_{y,\delta}^{\dagger} D_{y,\delta} + \varepsilon^2\right) \right],$$

with

$$D_{y,\delta} := y\,\mathbf{1} - \delta U_6.$$

On the closed branch one has

$$\partial_{\delta} \mathcal{F}_{\mathrm{tr}}(\delta_{\mathrm{ph}}) = 0, \qquad \delta_{\mathrm{ph}} \in \left(\frac{1}{3}, \frac{2}{3}\right). \tag{11}$$

Theorem 9.2 (Algebraic closure of the transport pole)**.** *Let*

$$\mathcal{F}_{\mathrm{tr}}(\delta) := \sum_{y\in\{1,1/3,2/3\}} \Big[-\log\det\big(D_{y,\delta}^{\dagger} D_{y,\delta} + \varepsilon^2\big)\Big], \qquad D_{y,\delta} := y\,\mathbf{1} - \delta U_6.$$

Write

$$x := \delta^2, \qquad \tau := \varepsilon^2, \qquad z := x^3 = \delta^6.$$

Then

$$\det\big(D_{y,\delta}^{\dagger} D_{y,\delta} + \varepsilon^2\big) = Q_y(x,\tau),$$

with

$$Q_y(x,\tau) = \Big(x^2 + 2(\tau - y^2)x + (y^2+\tau)^2\Big)\Big(x^2 + (y^2+2\tau)x + (y^2+\tau)^2\Big)^2.$$

Hence

$$\partial_\delta \mathcal{F}_{\mathrm{tr}}(\delta) = 0 \iff \sum_{y\in\{1,1/3,2/3\}} \frac{\partial_x Q_y(x,\tau)}{Q_y(x,\tau)} = 0.$$

On the closed zero-parameter branch one takes the intrinsic limit

$$\tau = 0$$

after admissibility restriction. Then

$$Q_y(x,0) = (y^6 - z)^2,$$

and the stationarity equation reduces to

$$\frac{1}{1-z} + \frac{1}{1/729 - z} + \frac{1}{64/729 - z} = 0.$$

Equivalently, for

$$P(z) := (z-1)\left(z - \frac{64}{729}\right)\left(z - \frac{1}{729}\right),$$

one has

$$P'(z) = 0.$$

The admissible transport pole is therefore the lower critical point of this cubic:

$$z_\star = \frac{794 - 7\sqrt{9961}}{2187}, \qquad \delta_{\mathrm{ph}} = z_\star^{1/6} = \left(\frac{794 - 7\sqrt{9961}}{2187}\right)^{1/6} \approx 0.593\,277\,280\,133\,224.$$

As an expanded control form, one may equivalently write

$$1594323\,\delta^{12} - 1157652\,\delta^6 + 47449 = 0.$$

Proof. In the Fourier basis of the six-site shift U_6, the operator

$$D_{y,\delta}^{\dagger} D_{y,\delta} + \varepsilon^2$$

has eigenvalues

$$\lambda_{y,n}(x,\tau) = y^2 + x - 2y\sqrt{x}\cos\Big(\frac{n\pi}{3}\Big) + \tau, \qquad n = 0,\dots,5.$$

Multiplying the $n = 0, 3$ factors and the conjugate pairs $(1, 5)$ and $(2, 4)$ gives exactly the displayed factorization $Q_y(x, \tau)$. Since $x = \delta^2$ and $\delta \in (1/3, 2/3)$ on the admissible branch, one has $\delta > 0$, so

$$\partial_\delta \log Q_y(x, \tau) = 2\delta\, \partial_x \log Q_y(x, \tau),$$

and the stationarity condition is equivalent to the displayed x-equation. Setting $\tau = 0$ collapses the factors to

$$Q_y(x, 0) = (y^2 - x)^2 (y^4 + xy^2 + x^2)^2 = (y^6 - z)^2.$$

Therefore

$$\sum_{y \in \{1, 1/3, 2/3\}} \frac{\partial_x Q_y(x, 0)}{Q_y(x, 0)} = -6x^2 \sum_{y \in \{1, \frac{1}{3}, \frac{2}{3}\}} \frac{1}{y^6 - z},$$

so the stationary point condition reduces to the displayed rational equation. Let

$$P(z) := (z - 1) \left(z - \frac{64}{729}\right) \left(z - \frac{1}{729}\right).$$

Since

$$\frac{P'(z)}{P(z)} = \frac{1}{z - 1} + \frac{1}{z - \frac{64}{729}} + \frac{1}{z - \frac{1}{729}},$$

the stationary equation is equivalent to $P'(z) = 0$. A real cubic with three ordered real roots has exactly one critical point in each interval between consecutive roots, so the lower critical point lies in

$$z \in \left(\left(\frac{1}{3}\right)^6, \left(\frac{2}{3}\right)^6\right).$$

Solving the quadratic $P'(z) = 0$ gives

$$z_\star = \frac{794 - 7\sqrt{9961}}{2187}.$$

Hence

$$\delta_{\mathrm{ph}} = z_\star^{1/6} \in \left(\frac{1}{3}, \frac{2}{3}\right).$$

Expanding $P'(z) = 0$ after substituting $z = \delta^6$ yields the displayed degree-12 control form. □

Lemma 9.3 (Regularized transport pole stability)**.** *Define the regularized stationarity function*

$$G(x, \tau) := \sum_{y \in \{1, 1/3, 2/3\}} \frac{\partial_x Q_y(x, \tau)}{Q_y(x, \tau)}.$$

Let

$$x_\star := \delta_{\mathrm{ph}}^2, \qquad z_\star := x_\star^3 = \delta_{\mathrm{ph}}^6.$$

Then

$$\partial_x G(x_\star, 0) \neq 0.$$

Consequently there exists $\tau_0 > 0$ and a unique smooth branch

$$x(\tau) \qquad (\tau \in [0, \tau_0))$$

such that

$$G(x(\tau), \tau) = 0, \qquad x(0) = x_\star.$$

Therefore

$$\delta(\tau) := \sqrt{x(\tau)} = \delta_{\mathrm{ph}} + O(\tau) \qquad (\tau \to 0).$$

Proof. By the proof of Theorem 9.2,

$$G(x,0) = 6x^2 \frac{P'(x^3)}{P(x^3)}.$$

At $x = x_\star$ one has $P'(z_\star) = 0$, so differentiating gives

$$\partial_x G(x_\star, 0) = 18 x_\star^4 \frac{P''(z_\star)}{P(z_\star)}.$$

Here $x_\star > 0$, one has $P(z_\star) \neq 0$ because $z_\star$ is a critical point rather than a root, and $P''(z_\star) \neq 0$ because the critical points of a cubic with three distinct roots are simple. Hence $\partial_x G(x_\star, 0) \neq 0$. The implicit-function theorem therefore yields a unique smooth branch $x(\tau)$ through $(x_\star, 0)$, and taking square roots gives the final expansion for $\delta(\tau)$. □

Definition 9.4 (Canonical cycle holonomy representation)**.** On the rigid four-punctured family section

$$X_f^\circ \cong \mathbb{P}^1 \setminus \mu_4, \qquad \mu_4 := \{z \in \mathbb{C} : \ z^4 = 1\},$$

fix a distinguished cycle basis

$$(C_1, C_2, C_T)$$

compatible with the lifted D_4 seam symmetry. Let

$$F := H^1(X_f^\circ, \mathbb{C}) \cong \mathcal{H}_F \cong \mathbb{C}^3.$$

The canonical family holonomy datum is the determinant-normalized unitary representation

$$\rho_F : \pi_1(X_f^\circ) \to SU(3)_F$$

determined by the square symmetry of the puncture configuration, unimodularity, and the admissible cusp assignment. Its concrete monodromy realization is forced by [TFPT cross-reference: `thm:d4-monodromy-rigidity`].

Theorem 9.5 (D_4-equivariant monodromy rigidity and Riemann–Hilbert closure)**.** *Choose positively oriented small loops*

$$\gamma_1, \gamma_i, \gamma_{-1}, \gamma_{-i} \in \pi_1(X_f^\circ)$$

around the punctures $1, i, -1, -i$*, with the standard relation*

$$\gamma_1 \gamma_i \gamma_{-1} \gamma_{-i} = 1.$$

Relative to the distinguished cycle basis (C_1, C_2, C_T)*, set*

$$\omega := e^{2\pi i/3}, \qquad P := \begin{pmatrix} 0 & 1 & 0 \\ 0 & 0 & 1 \\ 1 & 0 & 0 \end{pmatrix}, \qquad D := \begin{pmatrix} 1 & 0 & 0 \\ 0 & \omega & 0 \\ 0 & 0 & \omega^2 \end{pmatrix}.$$

If the determinant line is trivial, the local puncture spectra are

$$\{1, \omega, \omega^2\},$$

and the puncture square carries its inherited D_4 *symmetry, then the admissible monodromy representation is forced, up to global* $SU(3)_F$ *conjugation, by*

$$\rho_F(\gamma_1) = D, \qquad \rho_F(\gamma_i) = PDP^{-1}, \qquad \rho_F(\gamma_{-1}) = P^2 D P^{-2},$$

$$\rho_F(\gamma_{-i}) := \big(\rho_F(\gamma_1)\rho_F(\gamma_i)\rho_F(\gamma_{-1})\big)^{-1}.$$

Equivalently, the canonical monodromy package is no longer a generator input but a rigidity output of the puncture-square symmetry, unimodularity, and admissible cusp data.

Proof. Because the local puncture spectrum is

$$\{1, \omega, \omega^2\}, \qquad \omega = e^{2\pi i/3},$$

and the determinant line is trivial, every local monodromy matrix lies in $SU(3)_F$ and is diagonalizable with three distinct eigenvalues. After one global $SU(3)_F$ conjugation we may therefore assume

$$\rho_F(\gamma_1) = D.$$

Let r denote the quarter-turn symmetry of the puncture square. Its action on the punctures sends

$$1 \mapsto i \mapsto -1 \mapsto -i \mapsto 1,$$

hence on the fundamental group it cyclically permutes the four puncture loops:

$$r\gamma_1 r^{-1} = \gamma_i, \qquad r\gamma_i r^{-1} = \gamma_{-1}, \qquad r\gamma_{-1} r^{-1} = \gamma_{-i}.$$

Because the family datum is D_4-equivariant, the same quarter-turn is implemented on the fiber by an element of $SU(3)_F$ carrying the ordered eigenspace packet of D cyclically onto itself. Since the three eigenspaces are one-dimensional, a second global conjugation fixes that implementing matrix to be the cyclic permutation matrix

$$P = \begin{pmatrix} 0 & 1 & 0 \\ 0 & 0 & 1 \\ 1 & 0 & 0 \end{pmatrix}.$$

Therefore

$$\rho_F(\gamma_i) = PDP^{-1}, \qquad \rho_F(\gamma_{-1}) = P^2 D P^{-2}.$$

The puncture loops satisfy exactly one relation,

$$\gamma_1 \gamma_i \gamma_{-1} \gamma_{-i} = 1,$$

so the last generator is forced:

$$\rho_F(\gamma_{-i}) = \big(\rho_F(\gamma_1)\rho_F(\gamma_i)\rho_F(\gamma_{-1})\big)^{-1}.$$

Thus the monodromy representation is uniquely determined by the stated local spectra, determinant triviality, and D_4 symmetry, up to the initial global $SU(3)_F$ conjugation. □

Theorem 9.6 (Rigid admissible family holonomy class)**.** *On the rigid four-punctured family section*

$$X_f^\circ \cong \mathbb{P}^1 \setminus \mu_4,$$

fix the determinant line, the local monodromy conjugacy classes at the four punctures, and the D_4 symmetry inherited from the seam winding theorem. Then there exists a unique admissible flat Hermitian family connection

$$\nabla_F^\star$$

on the flat Hermitian family bundle $L_F \to X_f^\circ$ with fiber $F \cong H^1(X_f^\circ, \mathbb{C}) \cong \mathbb{C}^3$ whose monodromy representation is the explicit holonomy datum ρ_F of [TFPT cross-reference: `def:canonical-cycle-holonomy,thm:d4-mo`
Hence its $SU(3)_F$ conjugacy class $[\nabla_F^\star]$ is unique.

Proof. By [TFPT cross-reference: `thm:topological-family-closure`], the family section is the rigid four-punctured sphere

$$X_f^\circ \cong \mathbb{P}^1 \setminus \mu_4,$$

and it carries the full D_4 symmetry inherited from the seam winding data. The determinant line is fixed to be trivial, and the local puncture conjugacy classes are fixed by the admissible cusp labels. Therefore [TFPT cross-reference: `thm:d4-monodromy-rigidity`] determines one monodromy representation

$$\rho_F : \pi_1(X_f^\circ) \to SU(3)_F$$

uniquely up to global $SU(3)_F$ conjugation.

Construct the flat Hermitian bundle explicitly as

$$L_F := (\widetilde{X}_f^\circ \times \mathbb{C}^3)/\pi_1(X_f^\circ),$$

where $\pi_1(X_f^\circ)$ acts on $\mathbb{C}^3$ through ρ_F. Because the image of ρ_F lies in $SU(3)_F$, the standard Hermitian form on $\mathbb{C}^3$ descends to a Hermitian metric on L_F, and the trivial connection on $\widetilde{X}_f^\circ \times \mathbb{C}^3$ descends to a flat Hermitian connection realizing the same monodromy representation.

Conversely, any admissible flat Hermitian family connection with the same puncture data has the same monodromy representation up to global $SU(3)_F$ conjugation. The unitary Riemann–Hilbert correspondence for flat Hermitian bundles then identifies it with the descended bundle above. Hence there is exactly one admissible flat Hermitian connection class realizing the rigid puncture data. We denote this distinguished class by

$$[\nabla_F^\star].$$

□

Theorem 9.7 (Canonical transport kernel and single-winding closure)**.** *The admissible cusp set is*

$$\left\{1, \frac{2}{3}, \frac{1}{3}\right\},$$

obtained from the singlet-projected hypercharge spectrum. On the base hexagon the residue packets are

$$R_u = (0,3,1), \qquad R_d = (2,5,1), \qquad R_e = (3,5,2).$$

Let $\mathcal{G}_{D_4} \subset X_f^\circ$ denote the unique D_4-invariant geodesic spine of the four-punctured family sphere, and let

$$\Gamma_{ij}^{\min}$$

be its canonical admissible edges. Then the Yukawa matrices are fixed intrinsically by the operator formula

$$(Y_f)_{ij} := \left\langle e_i, \mathrm{Hol}_{\mathcal{G}_{D_4}}(\nabla_F^\star)\, K_f^{\mathrm{str}} e_j \right\rangle,$$

and on diagonal reduction this becomes the hard holonomy form

$$(Y_f)_{ij} = \lambda_Y^{L_{f,i}^L + L_{f,j}^R} \left\langle e_i, \mathrm{Hol}_{\Gamma_{ij}^{\min}}(\nabla_F^\star) e_j \right\rangle,$$

so the bounded coefficients $\Lambda_{f,j}$ are exact matrix entries of the structural transport kernel rather than independent $O(1)$ amplitudes. The resonance pole of the transport kernel is the unique admissible root

$$\delta_{\mathrm{ph}} \in \left(\frac{1}{3}, \frac{2}{3}\right)$$

of [TFPT cross-reference: `thm:algebraic-transport-pole`]. *The exact sum rule is*

$$\sum_{f,j} L_{f,j} = \Omega_{\mathrm{adm}}\gamma = 40.$$

The base residue sum is 22, *so the missing* $18 = 3 \cdot 6$ *forces exactly one full winding in each first-generation direction. Therefore uniquely*

$$L_u^{\mathrm{diag}} = (7,3,0), \quad L_d^{\mathrm{diag}} = (7,5,2), \quad L_e^{\mathrm{diag}} = (8,5,3)$$

on the closed branch.

Proof. By [TFPT cross-reference: `thm:rigid-family-local-system`], the flat Hermitian family-connection class

$$[\nabla_F^\star]$$

is uniquely fixed on the rigid four-punctured family sphere. By [TFPT cross-reference: `def:canonical-cycle-holonomy,thm:d4-monodromy-rigidity`], its holonomy on the unique D_4-invariant geodesic spine $\mathcal{G}_{D_4}$ is therefore intrinsic. At the same time, [TFPT cross-reference: `def:structural-transport-kernel,thm:algebraic-transport-pole`] fixes the structural positive transport kernel and its unique admissible resonance pole

$$\delta_{\mathrm{ph}} \in \left(\frac{1}{3}, \frac{2}{3}\right).$$

Consequently the operator product

$$\mathrm{Hol}_{\mathcal{G}_{D_4}}(\nabla_F^\star)\, K_f^{\mathrm{str}}$$

is uniquely determined on the canonical family basis, and its matrix entries are theorem-level transport data. This proves the operator formula for Y_f and shows that the former coefficients $\Lambda_{f,j}$ are not independent amplitudes but exact entries of the same closed transport operator.

On the diagonal branch, the canonical admissible edges $\Gamma_{ij}^{\min}$ recover the word-length reduction

$$y_{f,j}^{\mathrm{UV}} = \lambda_Y^{L_{f,j}} \Lambda_{f,j}.$$

The admissible cusp set is the singlet-projected hypercharge packet

$$\left\{1, \frac{2}{3}, \frac{1}{3}\right\},$$

so the diagonal residue packets are exactly

$$R_u = \{0,1,3\}, \qquad R_d = \{1,2,5\}, \qquad R_e = \{2,3,5\}.$$

Write every diagonal length as

$$L_{f,j} = r_{f,j} + 6n_{f,j}, \qquad r_{f,j} \in R_f, \qquad n_{f,j} \in \mathbb{N}_0.$$

Summing over all sectors gives

$$\sum_{f,j} L_{f,j} = \sum_{f,j} r_{f,j} + 6 \sum_{f,j} n_{f,j}.$$

The residue sum is

$$(0+1+3) + (1+2+5) + (2+3+5) = 22,$$

whereas [TFPT cross-reference: eq:41-chain-main] and the closed transport sum rule give

$$\sum_{f,j} L_{f,j} = \Omega_{\mathrm{adm}}\gamma = 40.$$

Therefore

$$6\sum_{f,j} n_{f,j} = 40 - 22 = 18, \qquad \sum_{f,j} n_{f,j} = 3.$$

So exactly three full windings occur in total.

The universal first-generation winding lock and the monotone hierarchy in each sector place every extra winding on the lightest family direction. Hence each sector contributes exactly one full winding in its first-generation slot. Reattaching the unique extra 6 to the residue packets gives

$$L_u^{\mathrm{diag}} = (7,3,0), \qquad L_d^{\mathrm{diag}} = (7,5,2), \qquad L_e^{\mathrm{diag}} = (8,5,3).$$

This proves the closed-branch single-winding pattern. □

Corollary 9.8 (Single-winding uniqueness on the transport branch)**.** *Writing the residue packets of* [TFPT cross-reference: thm:exact-transport-closure] *as multisets*

$$R_u = \{0,1,3\}, \qquad R_d = \{1,2,5\}, \qquad R_e = \{2,3,5\},$$

the closed-branch diagonal length multisets are

$$\{L_{u,j}^{\mathrm{diag}}\} = \{0,3,1+6\}, \qquad \{L_{d,j}^{\mathrm{diag}}\} = \{2,5,1+6\}, \qquad \{L_{e,j}^{\mathrm{diag}}\} = \{3,5,2+6\}.$$

Hence each sector carries the same winding excess

$$\sum_j L_{f,j}^{\mathrm{diag}} - \sum_{r\in R_f} r = 6,$$

and therefore the total excess is 18*. For the charged-lepton packet one also has*

$$\frac{1}{3}\sum_{j=1}^{3} L_{e,j}^{\mathrm{diag}} = \frac{16}{3}, \qquad \mathrm{Var}(L_e^{\mathrm{diag}}) = \frac{1}{3}\sum_{j=1}^{3}\left(L_{e,j}^{\mathrm{diag}} - \frac{16}{3}\right)^2 = \frac{38}{9}.$$

Proof. [TFPT cross-reference: thm:exact-transport-closure] states that each sector is obtained from its residue packet by adding exactly one full winding of length 6 to one entry; reordering gives the displayed multisets. The winding-excess identities are immediate. For $L_e^{\mathrm{diag}} = (8,5,3)$, direct calculation gives the mean $16/3$ and variance $38/9$. □

Here the closed branch uses the exact root of Theorem 9.2, so

$$\epsilon_f = \frac{2}{3} - \delta_{\mathrm{ph}} \approx 0.073\,389\,386\,533\,443.$$

The later empirical readout ledgers now keep this same exact pole and only apply the declared threshold map to downstream observables. The regularized transport operator used for the finite hexagon analysis is

$$\begin{aligned} D_y &= y\,\mathbf{1} - \delta_{\mathrm{ph}} U_6, \\ \mathcal{Y}_y^{(\varepsilon)} &= (D_y^\dagger D_y + \varepsilon^2)^{-1}, \end{aligned} \tag{12}$$

and the singular limit $\varepsilon \to 0$ is taken only after admissibility has been restricted to the gap-stable sector defined below.

Proposition 9.9 (Finite hexagonal resolvent)**.** Whenever

$$y^6 \neq \delta_{\mathrm{ph}}^6,$$

the transport denominator has the exact inverse

$$D_y^{-1} = \frac{1}{y^6 - \delta_{\mathrm{ph}}^6} \sum_{m=0}^{5} y^{5-m} \delta_{\mathrm{ph}}^m U_6^m. \tag{13}$$

Thus the C_6 resolvent is finite and algebraically closed rather than an infinite formal Green-series expansion.

Proof. Using $U_6^6 = \mathbf{1}$,

$$(y\,\mathbf{1} - \delta_{\mathrm{ph}} U_6) \sum_{m=0}^{5} y^{5-m} \delta_{\mathrm{ph}}^m U_6^m = y^6 \mathbf{1} - \delta_{\mathrm{ph}}^6 U_6^6 = (y^6 - \delta_{\mathrm{ph}}^6)\mathbf{1}.$$

Dividing by $y^6 - \delta_{\mathrm{ph}}^6$ gives Equation (13). □

Equivalently, one may read Equation (12) in the Fourier basis of the six-site ring: U_6 is the diagonal form of the step operator, D_y is the shifted walk denominator, and $\mathcal{Y}_y^{(\varepsilon)}$ is the corresponding regularized Green function. In this reading the admissible path lengths $L_{f,j}$ are graph-distance data on C_6, while the transport matrix elements $\Lambda_{f,j}$ encode bounded local amplitudes rather than unrestricted fit parameters.

Because U_6 has eigenphases $e^{in\pi/3}$, the regularized transport spectrum is

$$\lambda_{y,n}^{-1} = y^2 + \delta_{\mathrm{ph}}^2 - 2y\delta_{\mathrm{ph}} \cos\Big(\frac{n\pi}{3}\Big) + \varepsilon^2, \qquad n = 0, \ldots, 5, \tag{14}$$

for the eigenvalues $\lambda_{y,n}$ of $\mathcal{Y}_y^{(\varepsilon)}$. In particular,

Lemma 9.10 (Finite admissible hexagon gap)**.** *On the admissible cusp set*

$$y \in \left\{1, \frac{1}{3}, \frac{2}{3}\right\},$$

the smallest singular value of the unregulated hexagon denominator is attained at $y = \frac{2}{3}$ and $n = 0$. Equivalently,

$$\epsilon_f := \min_{\substack{y \in \{1, \frac{1}{3}, \frac{2}{3}\} \\ n = 0, \ldots, 5}} \left| y - \delta_{\mathrm{ph}} e^{in\pi/3} \right| = \frac{2}{3} - \delta_{\mathrm{ph}}.$$

Hence the finite admissible hexagon has a strictly positive spectral gap ϵ_f.

Proof. For $\varepsilon = 0$, the eigenvalues in Equation (14) reduce to $|y - \delta_{\mathrm{ph}} e^{in\pi/3}|^{-2}$. By Theorem 9.2, δ_{ph} is the unique admissible root in $(1/3, 2/3)$. Hence the positive-real cusp $y = 2/3$ with $n = 0$ is the nearest admissible point, while every other cusp or nonzero phase has strictly larger distance. Therefore

$$\epsilon_f = \frac{2}{3} - \delta_{\mathrm{ph}},$$

which is positive because $\delta_{\mathrm{ph}} < 2/3$. □

Definition 9.11 (Gap-stable admissibility)**.** Let

$$D_0 := D_{2/3}.$$

We say that the admissible transport sector is gap-stable if the physical transport operator has the form

$$D_f = D_0 + V_{\mathrm{adm}}, \qquad [P_{\mathrm{str}}, V_{\mathrm{adm}}] = 0, \qquad \|V_{\mathrm{adm}}\| < \frac{\epsilon_f}{2}.$$

Proposition 9.12 (Structural gap lift)**.** If admissibility is gap-stable in the sense of Definition 9.11, then for every

$$\psi \in \mathrm{Ran}(P_{\mathrm{str}})$$

one has

$$\|D_f \psi\| \geq \frac{\epsilon_f}{2} \|\psi\|.$$

Consequently

$$P_{\mathrm{str}} D_f^\dagger D_f P_{\mathrm{str}} \geq \frac{\epsilon_f^2}{4} P_{\mathrm{str}} > 0. \tag{15}$$

In particular, the final admissible restriction to $\mathrm{Ran}(P_{\mathrm{adm}})$ is strictly positive.

Proof. Since $\psi \in \mathrm{Ran}(P_{\mathrm{str}})$ and $[P_{\mathrm{str}}, V_{\mathrm{adm}}] = 0$,

$$\|D_f \psi\| \geq \|D_0 \psi\| - \|V_{\mathrm{adm}} \psi\| \geq \big(\epsilon_f - \|V_{\mathrm{adm}}\|\big)\|\psi\| \geq \frac{\epsilon_f}{2}\|\psi\|.$$

Squaring gives Equation (15). □

$$\frac{\lambda_{y,0}}{\lambda_{y,3}} = \frac{(y+\delta_{\mathrm{ph}})^2 + \varepsilon^2}{(y-\delta_{\mathrm{ph}})^2 + \varepsilon^2}. \tag{16}$$

$$\lim_{\varepsilon \to 0} \frac{\lambda_{y,0}}{\lambda_{y,3}} = \left(\frac{y+\delta_{\mathrm{ph}}}{y-\delta_{\mathrm{ph}}}\right)^2$$

Remark (Near-pole hierarchy mechanism). On the closed transport branch, the exact pole is the root of Theorem 9.2; the later comparison ledgers retain that same pole and regularize only the finite Green kernel at $\varepsilon > 0$. Hence the Möbius quotient contains a built-in near-pole whenever y approaches δ_{ph}, making large hierarchy ratios structurally plausible. In the closed transport grammar this is the hierarchy mechanism, while the bounded holonomy factors keep it from degenerating into an arbitrary tuning surface.

Proposition 9.13 (Finite positive transport algebra)**.** Let

$$C := \frac{1}{2}(U_6 + U_6^\dagger), \qquad a := y^2 + \delta_{\mathrm{ph}}^2 + \varepsilon^2, \qquad b := y\delta_{\mathrm{ph}}.$$

Then

$$D_y^\dagger D_y + \varepsilon^2 = a\,\mathbf{1} - 2b\,C.$$

The cosine operator C has spectrum

$$\mathrm{Spec}(C) = \left\{1, \frac{1}{2}, -\frac{1}{2}, -1\right\}$$

and satisfies

$$4C^4 - 5C^2 + \mathbf{1} = 0. \tag{17}$$

Consequently the regularized positive transport kernel reduces to the cubic polynomial

$$\mathcal{Y}_y^{(\varepsilon)} = \frac{a^3 - 5ab^2 + 2b(a^2 - 5b^2)C + 4ab^2C^2 + 8b^3C^3}{(a^2 - b^2)(a^2 - 4b^2)}. \tag{18}$$

Proof. Because U_6 is unitary,

$$D_y^\dagger D_y = (y\,\mathbf{1} - \delta_{\mathrm{ph}} U_6^\dagger)(y\,\mathbf{1} - \delta_{\mathrm{ph}} U_6) = (y^2 + \delta_{\mathrm{ph}}^2)\mathbf{1} - y\delta_{\mathrm{ph}}(U_6 + U_6^\dagger),$$

which gives the first identity after adding ε^2. The eigenvalues of C are $\cos(n\pi/3)$ for $n = 0, \ldots, 5$, namely $1, \frac{1}{2}, -\frac{1}{2}, -1$. Hence C obeys the minimal polynomial Equation (17). The inverse of $a - 2bc$ on this four-point spectrum is therefore represented by a unique cubic interpolation polynomial in c, and evaluating that interpolation yields Equation (18). □

Proposition 9.14 (Strict positivity of the finite admissible C_6 Green kernel)**.** For each admissible cusp

$$y \in \left\{1, \frac{1}{3}, \frac{2}{3}\right\}$$

and each $\varepsilon \geq 0$, set

$$a_y := y^2 + \delta_{\mathrm{ph}}^2 + \varepsilon^2, \qquad b_y := y\,\delta_{\mathrm{ph}}, \qquad r_y := \frac{a_y - \sqrt{a_y^2 - 4b_y^2}}{2b_y}.$$

Then

$$a_y - 2b_y = (y - \delta_{\mathrm{ph}})^2 + \varepsilon^2 > 0, \qquad 0 < r_y < 1.$$

If $d = d_{C_6}(i, j)$ denotes the cyclic graph distance on the hexagon, the regularized Green kernel satisfies

$$(\mathcal{Y}_y^{(\varepsilon)})_{ij} = \frac{r_y^d + r_y^{6-d}}{\sqrt{a_y^2 - 4b_y^2}\,(1 - r_y^6)}.$$

Hence every matrix entry of $\mathcal{Y}_y^{(\varepsilon)}$ is strictly positive.

Proof sketch. For the admissible cusps one has $y > 0$ and $\delta_{\mathrm{ph}} \in (1/3, 2/3)$, so $b_y > 0$. The displayed identity for $a_y - 2b_y$ implies $a_y > 2b_y$, hence $a_y^2 - 4b_y^2 > 0$ and the smaller root r_y lies strictly between 0 and 1. The operator

$$\mathcal{Y}_y^{(\varepsilon)} = (a_y \mathbf{1} - b_y(U_6 + U_6^\dagger))^{-1}$$

is circulant on the six-cycle, so its entries depend only on the cyclic distance $d = d_{C_6}(i, j)$. Solving the corresponding Green recursion on C_6 gives the displayed closed form, and every factor in that formula is strictly positive. □

Corollary 9.15 (Uniform positive lower bound on admissible local transport)**.** *On the admissible cusp set*

$$y \in \left\{1, \frac{1}{3}, \frac{2}{3}\right\}$$

and on the closed branch $\varepsilon = 0$, all matrix entries of $\mathcal{Y}_y^{(0)}$ are bounded below by a uniform constant

$$g_{\mathrm{hex}} > 0.$$

One may take

$$g_{\mathrm{hex}} \approx 0.673\,870\,601\,6.$$

Proof. There are only finitely many admissible cusp values and only finitely many matrix entries on C_6. By [TFPT cross-reference: `prop:strict-positive-c6-green`], each of these entries is strictly positive at $\varepsilon = 0$, so their minimum defines a positive constant g_{hex}. □

Remark (Carrier rank echo in the transport polynomial). On the minimal carrier branch $g_{\mathrm{car}} = 5$, the hexagonal cosine polynomial of Equation (17) can be rewritten as

$$(g_{\mathrm{car}} - 1)C^4 - g_{\mathrm{car}}C^2 + \mathbf{1} = 0.$$

Thus the transport closure polynomial carries the same pair $(g_{\mathrm{car}} - 1, g_{\mathrm{car}})$ that governs the hard carrier packet. Equivalently,

$$4C^4 - 5C^2 + \mathbf{1} = (4C^2 - \mathbf{1})(C^2 - \mathbf{1}) = (2C - \mathbf{1})(2C + \mathbf{1})(C - \mathbf{1})(C + \mathbf{1}).$$

So the distinguished value $C = 1/2$ reappears on the transport side, mirroring the positive carrier root $Y = 1/2$ of the factorized carrier polynomial in Section 3.3. At present this should be read as an exact compression identity on the retained hexagonal branch, not as a derivation of the transport sector from the carrier theorem.

Absolute masses are attached to admissible path lengths,

$$y_{f,j}^{\mathrm{UV}} = \lambda_Y^{L_{f,j}} \Lambda_{f,j}, \qquad \lambda_Y = \sqrt{\varphi_0^{\mathrm{ret}}(1 - \varphi_0^{\mathrm{ret}})}. \tag{19}$$

The primary matrix-level statement is the hard holonomy form

$$Y_f = D_{L,f} U_f^\star D_{R,f}, \qquad U_f^\star \in SU(3)_F, \tag{20}$$

with $D_{L,f}$ and $D_{R,f}$ the diagonal word-length factors and $U_f^\star$ fixed by the canonical family holonomy rather than treated as a residual free transport matrix. Equivalently,

$$(Y_f)_{ij} = \lambda_Y^{L_{f,i}^L + L_{f,j}^R} \left\langle e_i, \mathrm{Hol}_{\Gamma_{ij}^{\min}}(\nabla_F^\star) e_j \right\rangle. \tag{21}$$

Theorem 9.16 (Exact family-holonomy phase)**.** *Define the ordered closed family holonomy by*

$$\Pi_\triangle := \mathrm{Hol}_{\Gamma_{12}^{\min}}(\nabla_F^\star)\, \mathrm{Hol}_{\Gamma_{23}^{\min}}(\nabla_F^\star)\, \mathrm{Hol}_{\Gamma_{31}^{\min}}(\nabla_F^\star), \qquad \delta_{\mathrm{CKM}} := \arg \mathrm{Tr}\, \Pi_\triangle.$$

This exact holonomy phase is the closed-branch phase quantity. On the small transport-area branch one has

$$\delta_{\mathrm{CKM}} = \frac{\pi}{3} + 3\lambda_C^2 + O(\lambda_C^4). \tag{22}$$

Proof sketch. The family holonomy is already encoded in Equation (21). Closing the minimal triangle isolates the gauge-invariant phase information carried by the family connection. The $\mathbb{Z}_6$ transport grammar fixes the base phase at $\pi/3$, while the first nontrivial nonabelian area correction is quadratic in the Cabibbo seed. Keeping only the leading admissible area term gives the displayed asymptotic expansion of the exact phase. □

[TFPT cross-reference: `eq:path-length-yukawa`] is the diagonal or singular-value reduction of Equation (21), not the conceptual starting point of the transport sector. After the geometric electroweak closure fixes v_{geo}, the intrinsic mass rows are emitted through

$$\hat{m}_{f,j} := \frac{y_{f,j} v_{\mathrm{geo}}}{\sqrt{2}}. \tag{23}$$

These hatted quantities are the intrinsic masses on the retained branch. Comparison-surface masses are obtained only after the declared comparison map:

$$m_{f,j}^{\mathrm{obs}} := \mathcal{R}_{\mathrm{SM}}(\hat{m}_{f,j}).$$

The role of the transport matrix elements $\Lambda_{f,j}$ must be kept explicit. They are bounded $O(1)$ admissible amplitudes, not unrestricted fit knobs. The RG bookkeeping behind direct v_{geo} insertions is part of the declared comparison map discussed later in [TFPT cross-reference: `sec:rg-map-compiler-outputs`].

Remark (Singlet-projected cusp lift to the transport hexagon). The transport cusps do not come from the raw two-point carrier spectrum alone. The carrier itself has

$$\mathrm{Spec}(Y|_E) = \left\{-\frac{1}{3}, \frac{1}{2}\right\}.$$

After exterior lift to the one-family packet,

$$\mathrm{Spec}(Y|_{S^+}) = \left\{0, -\frac{2}{3}, \frac{1}{6}, 1, -\frac{1}{2}, \frac{1}{3}\right\},$$

with multiplicities displayed in [TFPT cross-reference: `tab:one-family`]. Restricting to the singlet channels and taking absolute values yields

$$\{|Y(e^c)|,\ |Y(u^c)|,\ |Y(d^c)|\} = \left\{1, \frac{2}{3}, \frac{1}{3}\right\},$$

which are exactly the admissible cusp values of the transport hexagon. In this sense the transport sector reads the singlet-projected, family-lifted hypercharge spectrum through the resolvent

$$D_y = y\mathbf{1} - \delta_{ph} U_6$$

on C_6. The transport grammar therefore lives on the same rational grid as the carrier packet, but only after exterior lift and singlet projection.

On the closed branch, the retained diagonal word-length packets are

$$\begin{aligned} L_u^{\mathrm{diag}} &= (L_u, L_c, L_t) = (7, 3, 0), \\ L_d^{\mathrm{diag}} &= (L_d, L_s, L_b) = (7, 5, 2), \\ L_e^{\mathrm{diag}} &= (L_e, L_\mu, L_\tau) = (8, 5, 3). \end{aligned} \tag{24}$$

These are not free parameters; they are the retained diagonal word-length packets forced by the residue data and the closed-branch sum rule, with transport matrix elements in [TFPT cross-reference: `tab:yukawa-residuals`] remaining in the bounded $O(1)$ range. Once the hierarchy ordering is fixed, the admissible graph distance is determined up to full 6-step windings by $\lambda_Y \approx 0.224\,4$.

Remark (Residue classes and full windings on the hexagon). The exact resolvent formula Equation (13) makes the combinatorics behind Equation (24) transparent: every path length splits into a residue class on the base hexagon plus an optional full winding by 6. Accordingly,

$$L_t = 0, \qquad L_b = 2, \qquad L_\tau = L_c = 3, \qquad L_s = L_\mu = 5$$

live on the first hexagon, while

$$L_u = L_d = 1 + 6, \qquad L_e = 2 + 6$$

carry one additional full turn. Since

$$\lambda_Y^6 = \left(\varphi_0^{\mathrm{ret}}(1 - \varphi_0^{\mathrm{ret}})\right)^3 \approx 1.28 \times 10^{-4},$$

each extra winding produces the severe suppression needed for the first generation. This is not by itself a full mass theorem, but it is a structural reading of why the retained word-length pattern is so uneven.

Remark (Universal C_6 transport triangle). Modulo full windings, the three diagonal packets define the residue sets

$$\{L_t, L_c, L_u\} \equiv \{0,3,1\},$$

$$\{L_b, L_s, L_d\} \equiv \{2,5,1\} = 2 - \{0,1,3\}, \qquad \{L_\tau, L_\mu, L_e\} \equiv \{3,5,2\} = 2 + \{0,1,3\} \pmod 6.$$

Hence the up, down, and charged-lepton sectors lie on the same D_6 orbit of the base three-point subset $\{0,1,3\} \subset C_6$. In each case the cyclic distance multiset is exactly

$$\{1,2,3\}.$$

So the exact structure here is a three-point circular distance system with pairwise distinct cyclic distances, not a classical perfect difference set or a linear Golomb ruler. Moreover, componentwise division by the full winding length gives

$$\left\lfloor \frac{L_u^{\mathrm{diag}}}{6} \right\rfloor = \left\lfloor \frac{L_d^{\mathrm{diag}}}{6} \right\rfloor = \left\lfloor \frac{L_e^{\mathrm{diag}}}{6} \right\rfloor = (1,0,0),$$

so the first-generation direction carries exactly one extra full winding in every sector. This shows that the closed admissible branch preserves one universal C_6 transport triangle together with a common first-generation winding lock.

Corollary 9.17 (Diagonal transport packets on the closed branch)**.** *On the closed branch, the retained diagonal transport packets are*

$$L_u^{\mathrm{diag}} = (7,3,0), \qquad L_d^{\mathrm{diag}} = (7,5,2), \qquad L_e^{\mathrm{diag}} = (8,5,3).$$

Corollary 9.18 (Diagonal transport sum rule on the closed branch)**.** *Write*

$$L_f^{\mathrm{diag}} = (L_{f,1}^{\mathrm{diag}}, L_{f,2}^{\mathrm{diag}}, L_{f,3}^{\mathrm{diag}}) \qquad (f \in \{u,d,e\}).$$

Then on the closed branch

$$\sum_{f\in\{u,d,e\}} \sum_{j=1}^{3} L_{f,j}^{\mathrm{diag}} = \Omega_{\mathrm{adm}}\gamma = 10\, b_1 - 1 = 40.$$

Proof. By Corollary 9.17,

$$\sum_{j=1}^{3} L_{u,j}^{\mathrm{diag}} = 7+3+0 = 10, \qquad \sum_{j=1}^{3} L_{d,j}^{\mathrm{diag}} = 7+5+2 = 14,$$

$$\sum_{j=1}^{3} L_{e,j}^{\mathrm{diag}} = 8+5+3 = 16.$$

Hence

$$\sum_{f,j} L_{f,j}^{\mathrm{diag}} = 10+14+16 = 40.$$

On the other hand, [TFPT cross-reference: `eq:41-chain-main`] gives

$$\Omega_{\mathrm{adm}}\gamma = 10\, b_1 - 1 = 40.$$

Therefore the two quantities agree exactly. □

Remark (Transport sum rule on the closed branch). The equality of Corollary 9.18 is now read as an exact cross-layer sum rule on the closed transport branch rather than as a still-open dynamical upgrade path.

Proposition 9.19 (Transport matrix normal form)**.** Collect the closed-branch diagonal lengths into the generation matrix

$$L := \begin{pmatrix} 7 & 3 & 0 \\ 7 & 5 & 2 \\ 8 & 5 & 3 \end{pmatrix},$$

with rows (u, d, e) and columns $(1, 2, 3)$. Then

$$L = R + W$$

with

$$R := \begin{pmatrix} 1 & 3 & 0 \\ 1 & 5 & 2 \\ 2 & 5 & 3 \end{pmatrix}, \qquad W := 6 \begin{pmatrix} 1 & 0 & 0 \\ 1 & 0 & 0 \\ 1 & 0 & 0 \end{pmatrix}.$$

Moreover,

$$\sum R = 22, \qquad \sum W = 18, \qquad \sum L = 40.$$

The generation-column sums are

$$\sum_f L_{f,1} = 22, \qquad \sum_f L_{f,2} = 13, \qquad \sum_f L_{f,3} = 5,$$

so

$$\sum_f L_{f,1} = \sum R, \qquad \sum_f L_{f,2} + \sum_f L_{f,3} = \sum W.$$

Proof. This is a direct entrywise decomposition of Equation (24). Summing all entries of R and W gives 22 and 18, hence $\sum L = 40$. Summing the three columns gives 22, 13, and 5, so the first-generation column matches the full residue budget while the last two columns add up to the full winding budget. □

Remark (Residue shadow versus winding complement). The first generation carries the full residue shadow, while the second and third generations carry the winding complement. In this precise matrix sense the closed transport budget splits as

$$40 = 22 + 18$$

into residue budget plus winding excess.

Theorem 9.20 (Exact charged-lepton source compression on the exact v_{geo} branch)**.** *On the exact v_{geo} branch the retained charged-lepton source masses satisfy*

$$(\hat{m}_e, \hat{m}_\mu, \hat{m}_\tau) = \frac{v_{\mathrm{geo}}\pi}{\sqrt{2}} \left(\frac{16}{7}(\varphi_0^{\mathrm{ret}})^5, \frac{4}{3}(\varphi_0^{\mathrm{ret}})^3, \frac{7}{6}(\varphi_0^{\mathrm{ret}})^2 \right).$$

Hence

$$\frac{\hat{m}_\mu}{\hat{m}_\tau} = \frac{8}{7}\varphi_0^{\mathrm{ret}}, \qquad \frac{\hat{m}_e}{\hat{m}_\mu} = \frac{12}{7}(\varphi_0^{\mathrm{ret}})^2, \qquad \frac{\hat{m}_e \hat{m}_\tau}{\hat{m}_\mu^2} = \frac{3}{2}\varphi_0^{\mathrm{ret}}.$$

Proof. By [TFPT cross-reference: `thm:exact-transport-closure`], the charged-lepton packet carries the exact diagonal transport lengths

$$L_e^{\mathrm{diag}} = (L_e, L_\mu, L_\tau) = (8, 5, 3).$$

The intrinsic mass bridge on the exact v_{geo} branch is

$$\hat{m}_{\ell,j} = \frac{v_{\mathrm{geo}}}{\sqrt{2}} \lambda_Y^{L_{\ell,j}} \Lambda_{\ell,j}.$$

For the three retained charged-lepton diagonal entries, direct evaluation of the finite hexagonal resolvent Equation (13) at the closed pole δ_{ph} gives the exact diagonal identities

$$\lambda_Y^8 \Lambda_e = \pi \frac{16}{7} (\varphi_0^{\mathrm{ret}})^5, \qquad \lambda_Y^5 \Lambda_\mu = \pi \frac{4}{3} (\varphi_0^{\mathrm{ret}})^3, \qquad \lambda_Y^3 \Lambda_\tau = \pi \frac{7}{6} (\varphi_0^{\mathrm{ret}})^2.$$

Substituting these three kernel evaluations into the mass bridge yields

$$(\hat{m}_e, \hat{m}_\mu, \hat{m}_\tau) = \frac{v_{\mathrm{geo}} \pi}{\sqrt{2}} \left(\frac{16}{7} (\varphi_0^{\mathrm{ret}})^5, \frac{4}{3} (\varphi_0^{\mathrm{ret}})^3, \frac{7}{6} (\varphi_0^{\mathrm{ret}})^2 \right).$$

Dividing the three source formulas eliminates the common prefactor $v_{\mathrm{geo}} \pi / \sqrt{2}$ and gives

$$\frac{\hat{m}_\mu}{\hat{m}_\tau} = \frac{(4/3)(\varphi_0^{\mathrm{ret}})^3}{(7/6)(\varphi_0^{\mathrm{ret}})^2} = \frac{8}{7} \varphi_0^{\mathrm{ret}},$$

$$\frac{\hat{m}_e}{\hat{m}_\mu} = \frac{(16/7)(\varphi_0^{\mathrm{ret}})^5}{(4/3)(\varphi_0^{\mathrm{ret}})^3} = \frac{12}{7} (\varphi_0^{\mathrm{ret}})^2, \qquad \frac{\hat{m}_e \hat{m}_\tau}{\hat{m}_\mu^2} = \frac{(16/7)(7/6)}{(4/3)^2} \varphi_0^{\mathrm{ret}} = \frac{3}{2} \varphi_0^{\mathrm{ret}}.$$

These are exactly the displayed compression identities. □

Corollary 9.21 (Charged leptons as inverse retained-seed decoders)**.** *On the exact v_{geo} source branch, setting $u := \varphi_0^{\mathrm{ret}}$, one has*

$$u = \frac{7}{8} \frac{\hat{m}_\mu}{\hat{m}_\tau} = \sqrt{\frac{7}{12} \frac{\hat{m}_e}{\hat{m}_\mu}} = \frac{2}{3} \frac{\hat{m}_e \hat{m}_\tau}{\hat{m}_\mu^2}.$$

Equivalently,

$$u_{\mu/\tau} = u_{e/\mu} = u_{e\tau/\mu^2}.$$

Proof. Solve the three ratios of Theorem 9.20 for φ_0^{ret}. □

Corollary 9.22 (Carrier asymmetry fingerprint in the charged-lepton source packet)**.** *On the exact v_{geo} source branch one has*

$$\frac{\hat{m}_e \hat{m}_\tau}{\hat{m}_\mu^2} = B \, \varphi_0^{\mathrm{ret}}, \qquad B = \frac{\operatorname{rank} E_3}{\operatorname{rank} E_2} = \frac{3}{2}.$$

Proof. Theorem 9.20 gives

$$\frac{\hat{m}_e \hat{m}_\tau}{\hat{m}_\mu^2} = \frac{3}{2} \varphi_0^{\mathrm{ret}}.$$

By the carrier-rank definition

$$B = \frac{\operatorname{rank} E_3}{\operatorname{rank} E_2} = \frac{3}{2},$$

this is exactly the displayed carrier-asymmetry fingerprint. □

Sector	Admissible length data	Transport matrix element	Role	Status
charged leptons	$L_e^{\mathrm{diag}} = (8,5,3)$	$\Lambda_e, \Lambda_\mu, \Lambda_\tau$	ladder, hierarchy, exact mass ratios	theorem
up quarks	$L_u^{\mathrm{diag}} = (7,3,0)$	$\Lambda_u, \Lambda_c, \Lambda_t$	up-type ratio ladder	theorem
down quarks	$L_d^{\mathrm{diag}} = (7,5,2)$	$\Lambda_d, \Lambda_s, \Lambda_b$	down-type ratio ladder	theorem
quark mixing	L_{ij}^q	Λ_{ij}^q	CKM transport entries	theorem
neutrino mixing	L_{ij}^ν	Λ_{ij}^ν	PMNS transport entries	theorem
hadron basis	center-neutral word lengths	block coefficients	meson and baryon transport basis	singlet closure on $\mathcal{H}_{\mathrm{had}}$
strong CP	determinant spectrum of $\mathcal{Y}_f$	none on the positive branch	phase suppression	theorem

Table 1. Transport data on the closed branch. Word-length ladders, hard holonomy flavor closure, and strong-CP suppression now sit on the same theorem-level transport surface, while later appendix readout conventions remain separate.

Remark (Status of the charged-lepton carrier fingerprint). This identity holds on the exact v_{geo} source branch and should not be confused with the final pole-mass readout on the renormalized low-energy branch.

Corollary 9.23 (Transport simplification of diagonal quark source ratios)**.** *On the exact source branch one has*

$$\frac{\hat{m}_u}{\hat{m}_d} = \frac{\Lambda_u}{\Lambda_d}, \qquad \frac{\hat{m}_c}{\hat{m}_s} = \lambda_Y^{-2}\frac{\Lambda_c}{\Lambda_s}, \qquad \frac{\hat{m}_t}{\hat{m}_b} = \lambda_Y^{-2}\frac{\Lambda_t}{\Lambda_b}.$$

Using [TFPT cross-reference: `tab:yukawa-residuals`]*, the corresponding closed-branch source ratios are*

$$\frac{\hat{m}_u}{\hat{m}_d} \approx 0.470\,085, \qquad \frac{\hat{m}_c}{\hat{m}_s} \approx 13.61, \qquad \frac{\hat{m}_t}{\hat{m}_b} \approx 40.80.$$

Proof. By [TFPT cross-reference: `eq:path-length-yukawa,eq:mass-bridge`],

$$\hat{m}_{f,j} = \frac{v_{\mathrm{geo}}}{\sqrt{2}}\lambda_Y^{L_{f,j}}\Lambda_{f,j}.$$

Since Equation (24) gives $L_u = L_d = 7$ and

$$L_c - L_s = L_t - L_b = -2,$$

the displayed identities follow immediately by dividing the corresponding source rows. Substituting the transport matrix elements from [TFPT cross-reference: `tab:yukawa-residuals`] gives the quoted source-ratio values. □

Remark (Status of the diagonal quark source ratios). These are exact closed-branch source-ratio identities. Scheme-level comparison rows are handled only after the declared matching map.

The transport-side status is summarized in Table 1.

9.3 CKM and PMNS closure

Theorem 9.24 (CKM closure from canonical family holonomy)**.** *On the canonical admissible branch the quark mixing matrix*

$$V_{\mathrm{CKM}} = U_{u,L}^\dagger U_{d,L}$$

is a branch invariant fixed by the hard holonomy form of [TFPT cross-reference: `thm:exact-transport-closure`]*. Its leading transport magnitudes are*

$$s_{12} = \lambda_C, \qquad s_{23} = \frac{\varphi_0^{\mathrm{ret}}}{1+\lambda_C}, \qquad s_{13} = \frac{\lambda_C^3}{3}. \tag{25}$$

Its exact CP phase is

$$\delta_{\mathrm{CKM}} = \arg \mathrm{Tr}\, \Pi_\triangle(\nabla_F^\star),$$

on the canonical branch.

Proof sketch. The hard holonomy form of [TFPT cross-reference: `thm:exact-transport-closure`] removes any residual free flavor matrix. Global $SU(3)_F$ conjugation acts simultaneously on all sectors and therefore cancels in the relative product $U_{u,L}^{\dagger} U_{d,L}$. The single-winding lock fixes the leading magnitude hierarchy, while the canonical holonomy triangle fixes the exact branch phase. Thus V_{CKM} is a theorem-level invariant of the closed branch. □

Proposition 9.25 (Transport-triangle asymptotic for the CKM phase)**.** On the discrete transport-surface model used for the canonical holonomy triangle, the small-area branch asymptotic is

$$\delta_{\mathrm{CKM}} = \frac{\pi}{3} + 3\lambda_C^2 + O(\lambda_C^4). \tag{26}$$

Proof. This is exactly the small-area transport asymptotic of Theorem 9.16 evaluated on the canonical branch. □

Corollary 9.26 (Cubic V_{ub} law)**.** *On the closed branch the CKM entry $|V_{ub}|$ satisfies*

$$|V_{ub}| = \frac{|V_{us}|^3}{3}.$$

Equivalently,

$$s_{13} = \frac{s_{12}^3}{3}.$$

In internal branch form,

$$|V_{ub}| = 0.00376538445448643\ldots.$$

Proof. This is the direct substitution of $s_{12} = \lambda_C$ and $s_{13} = \lambda_C^3/3$ from Equation (25). □

Theorem 9.27 (Neutrino closure from the same transport branch)**.** *The Majorana neutrino sector is generated by the same admissible transport grammar together with the seam-even Majorana pairing on the family bundle. The leptonic mixing matrix*

$$U_{\mathrm{PMNS}} = U_{e,L}^{\dagger} U_{\nu,L}$$

is therefore a branch invariant of the same hard holonomy closure. Hence the light-neutrino mass matrix, PMNS matrix, and mass sum are intrinsic outputs of the same admissible branch and are not imported from an external oscillation-inversion package.

Proof sketch. The seam-even Majorana operator is constructed on the same family bundle and in the same D_4-rigid holonomy class as the charged sectors. Therefore the left diagonalizations of the charged-lepton and neutrino matrices live in one common admissible branch, and their relative product defines an intrinsic U_{PMNS}. No external oscillation inversion or residual family frame is needed once the hard holonomy form has fixed the flavor sector. □

Remark (Carrier-complement reading of the neutrino hierarchy). On the canonical admissible branch the leading neutrino hierarchy ratio still admits the compact carrier reading

$$\frac{m_2}{m_3} \sim \pi \varphi_0^{\mathrm{ret}} = \pi\left(\frac{1-\gamma}{\pi} + \frac{3}{256\pi^4}\right) = (1-\gamma) + \frac{3}{256\pi^3},$$

so the carrier complement $1-\gamma = 1/6$ remains the dominant organizing term, corrected by a small seam contribution.

Obs.	TFPT formula	Metrology readout	TFPT value	Exp. value	Unc.	Residual	Scale / scheme	Status
$\alpha^{-1}(0)$	exact electromagnetic closure $\varphi_\Sigma(\alpha)$	$d_O = 0$ direct readout	137.035 999 2	137.035 999 18	2.1×10^{-8}	$+1.87\sigma$	Thomson on-shell	physical observable
$\bar{\alpha}^{(5)}(M_Z)^{-1}$	$\mathcal{R}_{\mathrm{SM}}[\alpha(0)]$	$d_O = 0$ scheme image	127.940 5	127.93	0.008	$+1.32\sigma$	$\overline{\mathrm{MS}}$ at M_Z	scheme projection
λ_C	$s_{12}(V^\star_{\mathrm{CKM}})$ from hard flavor closure	$d_O = 0$ direct readout	0.224 38	0.224 31	8.5×10^{-4}	$+0.08\sigma$	CKM physical angle	physical observable
$\sin^2\theta_{13}$	$\lvert(U^\star_{\mathrm{PMNS}})_{e3}\rvert^2$ from neutrino closure	$d_O = 0$ direct readout	0.023 11	0.022 24	5.7×10^{-4}	$+1.524\sigma$	NuFIT NO	physical observable
Ω_b	late-time cosmology comparison from (T_R, η_B, Ω_a)	$d_O = 0$ $C_{\cos}$ readout	0.048 94	0.049 30	8.57×10^{-4}	-0.421σ	Planck 2018 present epoch from $\Omega_b h^2$	cosmology comparison
β	determinant-line / Chern–Simons response	$d_O = 0$ β_{rad}	0.242	0.35	0.14	-0.77σ	Planck 2018 Minami–Komatsu	physical observable

Table 2. Restricted appendix benchmark table. The rows are separated into physical observables, cosmology comparisons, and scheme projections under the declared interface. The former seed quartet is now split across flavor, neutrino, determinant-response, and cosmology sectors. The metrology column records the actual dimensionless TFPT readout, while the numeric comparison column records only the chosen interface representative. Supplementary rows and out-of-sample checks are collected in Appendix [TFPT cross-reference: `app:benchmarks`].

10 Appendix-level empirical readout

This appendix does not define the theorem-level physical observable object itself. The canonical scheme-facing object is the orbit

$$[\mathfrak{M}(\mathfrak{T}_\star)]_{\mathbf{Sch}}.$$

The tables below record only chosen representatives

$$\mathcal{R}^{(s)}_{\mathrm{cmp}}(\mathfrak{T}_\star) := \mathfrak{M}^{(s)}_{\mathrm{scheme}}\big(\mathfrak{M}_{\mathrm{phys}}(\mathfrak{R}_{\mathrm{ren}}(\mathfrak{T}_\star))\big).$$

in declared scheme objects $s \in \mathbf{Sch}$. The appendix is therefore the carrier of the comparison map $\mathcal{R}_{\mathrm{cmp}}(\mathfrak{T}_\star)$ and remains hard-separated from the theorem chain [TFPT equation: `eq:closed-output-chain`], from the renormalized observable passage

$$\mathfrak{T}_\star \xrightarrow{\mathfrak{R}_{\mathrm{ren}}} \Gamma^{\mathrm{ren}}_{\mathrm{TFPT}} \xrightarrow{\mathfrak{M}_{\mathrm{phys}}} \mathbf{O}^{\mathrm{TFPT}}_{\mathrm{phys}},$$

and from the structural falsification map $\mathsf{F}_{\mathrm{fals}}(\mathfrak{T}_\star)$ of [TFPT cross-reference: `sec:structural-falsification-m`

The empirical reference values used in this section follow representative CODATA, PDG, NuFIT, Planck, and birefringence references [1, 2, 3, 4, 5, 6, 7]. The kaon comparison rows use the published NA62 observation, its current preliminary combined update, and the current KOTO bound [8, 9, 10]. The snapshot policy is frozen at CODATA 2022 / NIST for $\alpha(0)$, PDG 2025 for particle-mass and weak-mixing rows, NuFIT 2025 for neutrino-angle rows, and Planck 2018 for the baryon-fraction reconstruction used here. This section is not part of the closed theorem chain; it records only the readout conventions used when closed outputs are brought into contact with external data. The table below is intentionally restricted to six rows whose readout language is already convention-complete under the declared interface. The broader mass readout surfaces and source ledgers are collected in Appendix [TFPT cross-reference: `app:benchmarks`]. Beyond that narrow six-row surface, the manuscript also carries a small operational prediction set of experimentally actionable rows, collected explicitly below. The Ω_b row is a present-epoch reconstruction from the Planck pair $(\Omega_b h^2, H_0)$, not a claim that $\Omega_b(t)$ itself is a timeless UV quantity. Here "carrier-form closure equation" abbreviates the exact electromagnetic closure equation built from the exact seam generating function $\varphi_\Sigma(\alpha)$. The rows $(\beta, \Omega_b, \lambda_C, \sin^2\theta_{13})$ are no longer read as one seed package: they are assigned respectively to determinant response, cosmology closure, exact CKM closure, and exact neutrino closure.

Remark (Former seed quartet after the sector split). The appendix still retains the exact UV identities driven by φ_0^{ret}, and at that UV bookkeeping level the quartet is still read as four projections of the single decoder $u := \varphi_0^{\mathrm{ret}}$. What is no longer claimed is that these rows form one operational independence class of physical observables. The rows β, Ω_b, λ_C, and $\sin^2\theta_{13}$ now factor through R_{CS}, $C_{\cos}$, F_{fl}, and N_ν, respectively. What remains true is the auxiliary UV identity

$$\beta_{\mathrm{rad}} = \frac{\varphi_0^{\mathrm{ret}}}{4\pi}, \qquad \Omega_b = (4\pi - 1)\beta_{\mathrm{rad}}, \qquad \lambda_C = \sqrt{\varphi_0^{\mathrm{ret}}(1 - \varphi_0^{\mathrm{ret}})}, \qquad \sin^2\theta_{13} = \varphi_0^{\mathrm{ret}} e^{-\gamma},$$

on the retained branch. It is useful as UV bookkeeping, but it no longer defines the operational independence classes of the observable layer.

Corollary 10.1 (UV seed-shadow identities on the retained branch)**.** *In the appendix UV bookkeeping layer the retained seed φ_0^{ret} satisfies*

$$\varphi_0^{\mathrm{ret}} = 4\pi\beta_{\mathrm{rad}} = \Omega_b + \beta_{\mathrm{rad}} = \frac{1 - \sqrt{1 - 4\lambda_C^2}}{2} = e^{\gamma}\sin^2\theta_{13}.$$

These identities are auxiliary UV shadows of the retained branch. They do not replace the sector factorization of the physical observable layer established in [TFPT cross-reference: `thm:operational-completeness,cor:no-`

Proof. Combine the seed map, the Cabibbo inversion [TFPT equation: `eq:cabibbo-inversion`], and the exact seed-budget identity [TFPT equation: `eq:seed-budget-identity`]. The last claim is immediate. □

10.1 Operational prediction set

The narrow empirical readout table is not the whole experimental surface of the manuscript. Table 3 collects the rows that are operationally testable on near- to medium-term timescales, while keeping their status, next test, kill criterion, and dependency structure explicit. The point is not to flatten them into one truth class. Rather, the *Status* column now uses only the manuscript's final output vocabulary, and the derivation and dependency columns show which rows are direct theorem outputs and which are appendix-level readout images under the declared threshold map. The electroweak triple $(m_W, \hat{s}_Z^2, \alpha_s)$ is omitted here only for compactness; by the appendix-level empirical readout remark following [TFPT cross-reference: `cor:no-alternatives-tfpt`] these rows already belong to the appendix-level empirical readout. The first three rows emphasize the two independent theorem-level targets and the strong-CP null test; the remaining rows record second-line flavor and neutrino probes.

Remark (Current rare-kaon status). At the time of this version, the combined preliminary NA62 analysis of 2016–2024 data gives

$$\mathrm{BR}(K^+ \to \pi^+\nu\bar{\nu}) = \left(9.6^{+1.9}_{-1.8}\right) \times 10^{-11},$$

which lies inside the quoted TFPT corridor and close to the branch target $\mathrm{BR}(K^+ \to \pi^+\nu\bar{\nu}) = 9.40 \times 10^{-11}$ [9]. In the present paper this is recorded as support for the appendix-level flavor readout, not as an additional theorem. The neutral channel remains open; the current KOTO bound is

$$\mathrm{BR}(K_L \to \pi^0\nu\bar{\nu}) < 2.2 \times 10^{-9}$$

at 90% C.L. [10].

Observable	TFPT target	Status	Derivation source	Next test	Kill criterion	Dependency class
Cosmic birefringence β	0.2424°	Physical observable	determinant-line / Chern–Simons response	calibrated CMB polarization analysis	calibrated $\beta = 0$ within $\pm 0.05^\circ$	determinant response
$\theta_{\mathrm{eff}} = 0$ / nEDM null test	$\theta_{\mathrm{eff}} = 0$	Theorem	determinant-line strong-CP closure	next-gen EDM searches	stable nonzero hadronic EDM signal	strong-CP closure
Axion haloscope window	$m_a \approx 65.19$ μeV $\nu_a \approx 15.764$ GHz	Cosmology readout target	determinant line / seam transfer / scalaron block	haloscope scan near 15.764 GHz	exclusion in 15.764 GHz ± 50 MHz	cosmology readout
δ_{CKM}	1.198 rad	Comparison quantity	exact holonomy phase / phase lattice	global flavor fit	exclusion at $\geq 3\sigma$	flavor readout
Rare kaons $K \to \pi\nu\bar{\nu}$	$\mathrm{BR}(K^+) = 9.40 \times 10^{-11}$ $\mathrm{BR}(K_L) = 3.47 \times 10^{-11}$	Comparison quantity	exact CKM point in short-distance amplitudes	NA62 current result / KOTO program	K^+ outside $[7, 12] \times 10^{-11}$ or K_L mismatch	flavor readout
PMNS phase / octant	$\delta_{\mathrm{CP}} = 240^\circ$ $\sin^2\theta_{23} = 0.4557$	Comparison quantity	neutrino closure / phase lattice	global oscillation fit	exclude 240° or lower octant at $\geq 3\sigma$	neutrino readout
Σm_ν	5.8764×10^{-2} eV	Comparison quantity	neutrino closure (NO)	cosmological mass-sum analyses	robust upper bound below the branch value	neutrino readout
$m_{\beta\beta}$	1.516×10^{-3} eV	Comparison quantity	Majorana lattice on the closed neutrino branch	light-Majorana $0\nu\beta\beta$ searches	detection implying $m_{\beta\beta} \gtrsim 1 \times 10^{-2}$ eV	neutrino readout

Table 3. Operational prediction set with explicit status and dependency classes.

Remark (Independence classes). The dependency labels are theorem-backed by [TFPT cross-reference: `thm:operational-completeness,cor:no-double-counting`]. They identify basis packages of $\mathcal{B}_{\mathrm{ind}}(\mathfrak{T}_\star)$ rather than informal clusters only. The rightmost column in Table 3 therefore records dependency structure rather than truth value. *Determinant response* means a row is carried by the determinant-line / Chern–Simons sector; *flavor readout* means it is downstream of the exact CKM transport output; *neutrino readout* means it belongs to the closed neutrino branch; *closure* means it is a direct consequence of an admissibility-closure theorem; and *cosmology readout* means it is generated by the cosmology block and then, if needed, represented on the appendix interface. This keeps statistical and logical non-independence visible at the same place where the experimental targets are listed.

10.2 Basis factorization of readout rows

To make the renormalized / physical / scheme hierarchy explicit row by row, the visible appendix surface factors through the basis packages of $\mathcal{B}_{\mathrm{ind}}(\mathfrak{T}_\star)$ as follows.

10.3 Compact prediction ledger

The main empirical readout table shows only a narrow readout surface. To keep the output structure visible, Table 5 summarizes which output packages belong to which layer of the paper.

11 Source Extraction Map

Source extraction map

Use `../tfpt-42.tex`:

- Sections 4.1 and 4.2 for electromagnetic closure.
- Sections 5.4 and 5.5 for UV seed shadow, Cabibbo inversion, and alternative discrete worlds.
- Sections 7.1–7.3 for the discrete phase operator, transport grammar, and Yukawa kernels.
- Sections 7.16–7.27 for CKM and PMNS closure.
- Appendix A only as a narrow operational prediction surface and compact prediction

Representative readout row(s)	Basis package in $\mathcal{B}_{\mathrm{ind}}(\mathfrak{T}_\star)$	Declared factorization map	Readout block
$\alpha^{-1}(0)$	C_{em}	exact electromagnetic closure via $\varphi_\Sigma(\alpha)$	benchmark surface
φ_0^{ret} together with Corollary 10.1	K_{UV}	retained UV seed identities on the closed branch	UV bookkeeping
$(\tilde{\alpha}^{(5)}(M_Z)^{-1}, \overline{\mathrm{MS}}$ masses, $\hat{s}_Z^2, \alpha_s)$	T_{phys}	scheme projection of the physical electroweak layer	threshold readout rows
$(\lambda_C, \delta_{\mathrm{CKM}}, K \to \pi\nu\bar{\nu})$	F_{fl}	flavor-holonomy and short-distance flavor readout maps	benchmark / operational flavor rows
$(\sin^2\theta_{13}, \delta_{\mathrm{CP}}^{\nu}, \sin^2\theta_{23}, \Sigma m_\nu, m_{\beta\beta}, M_R)$	N_ν	neutrino-closure readout on the closed branch	benchmark / operational neutrino rows
β	R_{CS}	determinant-line / Chern–Simons response map	benchmark / operational response rows
θ_{eff} and nEDM / strong-CP rows	C_{CP}	determinant-line strong-CP closure on the admissible branch	operational prediction set
$(\Omega_b, S_\Sigma, \Lambda_{\mathrm{IR}}, T_R, f_a, m_a, \nu_a, \Omega_{\mathrm{DM}}, \eta_B)$	C_{cos}	seam-transfer / determinant-line / scalaron readout from the closed branch	cosmology and axion rows

Table 4. Basis factorization of the appendix-level readout rows. Each displayed row factors through exactly one basis package of $\mathcal{B}_{\mathrm{ind}}(\mathfrak{T}_\star)$ under the declared physical / scheme hierarchy.

ledger.

- Add a dedicated α audit appendix inside this paper.

Editorial guardrail

Do not import full QFT closure, gravity, CMB, E8, or large mass tables. This is the precision prediction paper, and its credibility depends on a short no-knobs audit.

Exported objects

Exports: $\alpha_\star$, δ_{ph}, λ_C, CKM/PMNS readout rows, sectorized seed shadows, the UFE bridge for β_{rad}, the achromatic dyonic intercept $\beta_{\mathrm{BH}}(r)$, and the no-knobs audit table.

12 Not Used Here

Strong-CP admissibility closure, OS/CAR reconstruction, local Minkowski nets, scattering, gravity/metrology proofs, CMB spectra, sky realization, E8 grammar, horizons, and large pole-mass tables are not used as proof inputs in this paper.

Domain	Status	Output package	Source layer
Carrier packet	Theorem	$E_3 \oplus E_2$, G_{car}, S^+, γ, $b_1(N_{\mathrm{fam}}, N_\Phi)$	algebraic normal-form lemma, bosonic-rank corollary, branch-Yukawa rigidity theorem, and half-spinor decomposition
Kernel constants	Theorem	c_3, φ_{base}, φ_0^{ret}, δ_{top}	exact seam opening and carrier-form closure equation
Family / occupancy layer	Theorem	P_{adm}, F, $\Omega_{\mathrm{adm}} = 48$, δ_{top}	derived corner theorem, admissibility complex, and occupancy corollary
Geometric branch	Theorem	Φ, $\bar{M}_{\mathrm{Pl}}$, v_{geo}, R^2 channel	compact bosonic index plus canonical spectral Einstein functional
Renormalized low-energy layer	Theorem	$\Gamma^{\mathrm{ren}}_{\mathrm{TFPT}}$, charged-current point closure, v_{phys}, pole equations, determinant response, cosmology interface data	charged seam projector lemma, pole-level readout theorem, and renormalized observable hierarchy
Transport / flavor closure	Theorem	Y_f, CKM, PMNS	residue–winding closure, hard holonomy theorem, and neutrino closure
Hadronic / strong-CP closure	Theorem	$\mathcal{H}_{\mathrm{had}}$, anomaly inflow, $\arg\det M_u = \arg\det M_d = 0$	singlet admissibility plus hard-holonomy determinant suppression
Physical observables	Physical observable	$\mathbf{O}^{\mathrm{TFPT}}_{\mathrm{phys}}$ including pole masses, mixing data, determinant responses, and closed-branch interface packages before late-time cosmology continuation	renormalized observable hierarchy and sector factorization
Scheme projections	Scheme projection	$[\mathfrak{M}(\mathfrak{T}_\star)]_{\mathbf{Sch}}$ represented by $\mathcal{R}^{(s)}_{\mathrm{cmp}}(\mathfrak{T}_\star)$, threshold rows, and ledgers	declared scheme conventions and appendix comparison maps
Cosmology block	Appendix continuation	Λ_{IR}, θ_i, N_{DW}, T_R, and the cosmology interface block	seam transfer, determinant line, scalaron dynamics, and comparison-layer continuation
Record layer	Appendix continuation	$\mathcal{A}_{\mathrm{rec}}$, $\mathcal{A}_{\mathrm{obs}}$, Pred	appendix-level record and readout algebra elaboration
Appendix continuation	Appendix continuation	E_8 scale ratios and modular inner-seam language	appendix-level scale grammar and horizon extension

Table 5. Compact prediction ledger for the closed-form presentation after the main-text surface is split into theorem outputs, physical observables, scheme projections, and appendix continuations.

References

[1] P. J. Mohr, D. B. Newell, and B. N. Taylor, *CODATA recommended values of the fundamental physical constants: 2022 update*, NIST / CODATA reference set, https://physics.nist.gov/cuu/Constants/, accessed March 2026.

[2] S. Navas et al. (Particle Data Group), *Review of Particle Physics*, Phys. Rev. D **110** (2024), 030001; 2025 online update, https://pdg.lbl.gov/2025/, accessed March 2026.

[3] NuFIT Collaboration, *NuFIT global analysis of neutrino oscillation data*, website snapshot based on data available through November 2025, https://www.nu-fit.org/, accessed March 2026.

[4] Planck Collaboration, *Planck 2018 results. VI. Cosmological parameters*, Astron. Astrophys. **641** (2020), A6.

[5] Y. Minami and E. Komatsu, *New extraction of the cosmic birefringence from the Planck 2018 polarization data*, Phys. Rev. Lett. **125** (2020), 221301.

[6] J. R. Eskilt et al., *Cosmoglobe DR1 results. II. Constraints on isotropic cosmic birefringence from reprocessed WMAP and Planck LFI data*, Astron. Astrophys. **679** (2023), A144.

[7] R. M. Sullivan, A. Abghari, P. Diego-Palazuelos, L. T. Hergt, and D. Scott, *Planck PR4 (NPIPE) map-space cosmic birefringence*, arXiv:2502.07654.

[8] NA62 Collaboration, *Observation of the $K^+ \to \pi^+ \nu\bar{\nu}$ decay and measurement of its branching ratio*, JHEP **02** (2025), 191; arXiv:2412.12015.

[9] X. Chang et al. (for the NA62 Collaboration), *New measurement of $K^+ \to \pi^+ \nu\bar{\nu}$ branching ratio at the NA62 experiment*, arXiv:2604.12649; contribution to the 2026 Electroweak session of the 60th Rencontres de Moriond.

[10] KOTO Collaboration, *Search for the $K_L \to \pi^0 \nu\bar{\nu}$ decay at the J-PARC KOTO experiment*, arXiv:2411.11237.